PUBLISHING HOUSE «ACADEMY OF NATURAL HISTORY»

Modern Problems of Science and Education. Surgery

Online peer-reviewed scientific journal

ISSN 2686-9101

№ 3 2020

Translated version of the surgery section of the Russian journal "Modern problems of science and education"
ISSN 2070-7428 www.science-education.ru

Editorial office
Post address: 101000,
Moscow, PO box 47
Edition Tel/Fax
+7 (499) 704-13-41
e-mail: edition@rae.ru

Founder: Academy Of Natural History, LLC.
440026, Russia, Penza,
3, Lermontoava str.
Founder Tel / Fax
+7 (499) 704-13-41
e-mail: edition@rae.ru

www.clinical-medicine.ru

Modern Problems of Science and Education. Surgery
www.clinical-medicine.ru

СОДЕРЖАНИЕ

DYNAMICS OF MARKERS OF STRUCTURAL AND FUNCTIONAL STATE OF THE ENDOTHELIUM IN SUBCUTANEOUS IMPLANTATION OF SCAFFOLDS OF POLYCAPROLACTONE AND VATERITE

Ivanov A.N.[1], Chibrikova Yu.A.[2], Norkin I.A.[1]

[1]Research Institute of Traumatology, Orthopedics and Neurosurgery of Saratov State Medical University named after V.I. Razumovsky of Ministry of Health of the Russian Federation, Saratov, e-mail: lex558452@rambler.ru;

[2]Saratov State Medical University named after V.I. Razumovsky, Saratov

Aims

The aim of this work was to evaluate the dynamics of markers of the structural and functional state of the endothelium in subcutaneous implantation of scaffolds of polycaprolactone and vaterite as compared to non-biocompatible matrices.

Materials and Methods

In the experiment in albino rats, the changes in serum concentrations of C-reactive protein, vascular endothelial growth factor, syndecan 1 and VE-cadherin were studied in the subcutaneous implantation of scaffolds of polycaprolactone and vaterite compared to non-biocompatible matrices.

Results

It has been established that the absence of biocompatibility of scaffolds is manifested as a systemic inflammatory response and prolonged proangiogenic activity accompanied by the formation of an inflammatory phenotype of endotheliocytes. In the implantation of scaffolds of polycaprolactone, the pattern of systemic inflammatory response is consistent with that of sham operated animals, indicating biocompatibility of these matrices. The increase in vascular endothelial growth factor concentration soon after implantation, in the absence of evidence of endothelial glycocalyx damage, characterises the high angiogenic potential of the scaffolds of polycaprolactone and vaterite.

Conclusions

The most informative element for predicting vascularisation of scaffolds in subcutaneous implantation tests is the ratio of the change in serum concentrations of vascular endothelial growth factor and syndecan 1, which enables the evaluation of the angiogenic potential of the matrix from the seventh day after subcutaneous implantation until the morphological evidence of new vessel formation.

Keywords: scaffolds, vascularisation, endothelium, inflammation, regeneration.

INTRODUCTION

Today's regenerative medicine sees prospects in 3D scaffolds that function as intercellular matrices to support the migration, proliferation, and directed differentiation of cells, thus accelerating the reparation processes [1]. Regeneration requires adequate tissue nourishment, which in the case of 3D matrices is enabled by vessels growing into the scaffold [2]. With respect to scaffolds used to stimulate the regeneration of bone tissue, what makes intra-matrix vessels so important is the multifaceted role vessels play in the migration of osteoclasts and osteoblasts, as well as in the mineralization of the newly formed bone tissue and its subsequent remodeling. If new vessels fail to emerge in the scaffold, it will hinder osteogenesis, i.e. reduce the osteoinductive properties of the implanted matrix [3]. Therefore, the angiogenic characteristics of the scaffold contribute substantially to its osteoinductive properties and the general regenerative potential alike. This is why the current situation calls for research into the vascularization of mineral-based matrices and the factors regulating the process, as such research will help predict and modulate the regeneration-boosting properties of scaffolds.

Regardless of the application, scaffolds must be biocompatible [4]. The intensity, duration, and specifics of the inflammatory response to implanting are the key indicators of biocompatibility. Notably, some inflammation mediators induce angiogenesis, thus being crucial to the effective scaffold vascularization. At the same time, intense inflammation inhibits scaffold vascularization and cellular population [5].

Angiogenic reactions are based on the migration and proliferation of endothelial cells. For this study, research into how scaffold biocompatibility and structural/functional endothelial changes correlate is of theoretical and practical interest, in particular with respect to the predictive value of the markers of angiogenic reactions in endothelial cells, which is what defines the focus of this research.

The research goal is to evaluate the dynamics of the structural and functional endothelial markers as affected by subcutaneous implantation of polycaprolactone and vaterite scaffolds in comparison to non-biocompatible matrices.

MATERIAL AND METHODS

The research design involved 54 animals split at random into four groups: control (8 rats), comparison (12 sham-operated rats), negative control (17 rats with the implanted non-biocompatible scaffolds: polycaprolactone matrices containing native ovalbumin), and experimental (17 animals with the implanted polycaprolactone and vaterite scaffolds). Pursuant to the guidelines of Razumovsky Saratov State Medical University's Ethics Committee (Minutes No. 6 of February 6, 2018), invasive manipulations on rats were performed with general anesthesia carried out by combined intramuscular administration of xylazine (Interchemie, the Netherlands), and telazol (Zoetis, Spain). Rats were sacrificed by overdosing these medications.

The implanted matrices were made by the Education and Research Institute of Nanostructures and Biosystems. Subcutaneous implantation tests lasting 7 or 21 days were run following the method described in [4, 6]. On Days 7 or 21, the cardiac puncture was performed to sample 5 ml of blood to produce serum.

ELISA tests were used to detect the following in the experimental animals' serum: C-reactive protein (CRP) with the Rat C-Reactive Protein ELISA kits (eBioscience, USA) to evaluate the systemic inflammatory response; vascular endothelial growth factor (VEGF) with the Rat VEGF Immunoassay (R&D Systems, USA) to evaluate angiogenesis-regulating mechanisms; soluble forms of syndecan-1 and VE-cadherin with the ELISA Kit for Syndecan 1 Rat and ELISA Kit for Cadherin 5 Rat (CloudClone Corp, USA) to evaluate damage sustained by endotheliocyte glycocalyx and the stability of the microvascular bed. ELISA tests were run on an Anthos 2020 microplate reader (Biochrom, UK) exactly as instructed by the kit manufacturers.

The collected data were processed statistically in Statistica 10.0 software and presented as median and interquartile ranges because the data were not normally distributed. Mann-Whitney tests were run for pairwise comparison to calculate the confidence level (p=0.05 as the threshold).

RESULTS

The research found out that on Day 7 of subcutaneous matrix implantation, the comparison rats had their CRP level increased by 18.7%. CRP in sham-operated animals did not differ significantly from that in intact animals by Day 21, see the Table.

On Day 7, the comparison rats had a 1.7 times higher VEGF concentration than the controls, a sign of proangiogenic activity induced by tissue injury. By Day 21 after the surgeries, VEGF levels in the comparison animals normalized and did not differ significantly from that in the controls, a sign of active angiogenesis being over. On Days 7 and 21 after the sham surgeries, comparison rats did not have significantly different concentrations of soluble endothelial cell glycocalyx components compared to the controls, see the Table. Therefore, implantation-free surgery induced a transient mild increase in CRP and VEGF concentrations in blood as recorded on Day 7. Normalization of the biochemical parameters by Day 21 indicated the completion of angiogenic processes and the stabilization of the vascular bed; it also corresponded to the lack of systemic inflammatory response signs. This is in line with the earlier findings of the dynamic microcirculatory-bed blood flow monitoring and with the morphological characteristics of surgeries in the scope of subcutaneous implantation testing [6].

In negative controls, CRP concentration rose on Day 7 after implanting non-biocompatible ovalbumin-impregnated scaffolds; the difference was significant against the controls and the sham-operated rats alike. On Day 21, CRP concentration dropped in negative controls compared to Day 7 values; however, it was still 1.25 times and 1.17 times higher than that of intact and sham-operated animals, respectively, see the Table.

Table 1

Concentration of the structural and functional endothelial markers in the experimental animals' serum

Groups	CRP, mg/l	VEGF, pg/ml	Syndecan-1, ng/ml	VE-cadherin, pg/ml
Controls (n=8)	101 (96; 114)	9.4 (7.3; 15.7)	1.11 (0.82; 1.51)	56.18 (54; 60.54)
Comparison group, Day 7 (n=6)	120 (118; 126) p1<0.05	16.2 (14.7; 18.8) p1<0.05	1.45 (0.91; 1.88) p1>0.05	56.18 (54; 60.55) p1>0.05
Comparison group, Day 21 (n=6)	108 (106; 117) p1>0.05 p2>0.05	8.9 (7.3; 12.6) p1>0.05 p2>0.05	1.2 (0.97; 1.84) p1>0.05 p2>0.05	57.27 (54; 60.55) p_1>0.05 p_2>0.05
Negative controls, Day 7 (n=8)	168 (131; 203) p1<0.05 p3<0.05	30.8 (26.1; 34.4) p1<0.05 p3<0.05	2.31 (1.91; 2.67) p1<0.05 p3<0.05	60.55 (54; 62.73) p1>0.05 p3<0.05
Negative control, Day 21 (n=9)	127 (125; 129) p_1<0.05 p_2<0.05 p_3<0.05	54.2 (23; 69.2) p_1<0.05 p_2>0.05 p_3<0.05	2.3 (1.96; 2.4) p_1<0.05 p_2>0.05 p_3<0.05	58.4 (56.2; 62.6) p_1>0.05 p_2>0.05 p_3>0.05
Experimental group, Day 7 (n=8)	126 (108; 129) p1<0.05 p3>0.05 p4<0.05	50 (32.3; 66.2) p1<0.05 p3<0.05 p4<0.05	1.31 (1.11; 1.78) p1>0.05 p3>0.05 p4<0.05	57.2 (52.9; 60.55) p1>0.05 p3>0.05 p4>0.05
Experimental group, Day 21 (n=9)	106 (102; 109) p_1>0.05 p_2>0.05 p_3>0.05 p_4<0.05	11.5 (9.5; 16.7) p_1>0.05 p_2<0.05 p_3>0.05 p_4<0.05	1.37 (0.63; 2.04) p_1>0.05 p_2>0.05 p_3>0.05 p_4<0.05	57.3 (53; 62.7) p_1>0.05 p_2>0.05 p_3>0.05 p_4>0.05

Note: The results are shown as the median and the interquartile range. $p_{1,2,3,4}$ are statistical significance values of the difference against the controls, Day 7 data, the comparison group, and the negative control on the same day, respectively.

A systemic inflammatory response featuring a higher CRP concentration in blood might be due to local leukocyte infiltration of the ovalbumin-impregnated matrix itself and its perifocal zone as discovered by earlier morphological studies [7]; this infiltration is associated with a hyperproduction of proinflammatory cytokines and indicates the non-biocompatibility of the scaffold. Negative controls had 1.9 times higher VEGF concentration than that of the comparison rats on Day 7, see the Table. By Day 21, non-biocompatible matrices tended to further increase in VEGF concentration, a sign of prolonged and pronounced activation of angiogenesis. Literature data suggest that prolonged hyperproduction of VEGF does not lead to scaffold vascularization; it is likely associated with the vascularization of the growing connective tissue that creates a separating barrier around the matrix [5]. Therefore, increase blood levels of VEGF persisting up to 21 days after subcutaneous implantation testing are not a favorable condition for scaffold vascularization.

No significant change in the concentration of VE-cadherin was identified in the negative controls. On Day 7 and Day 21 alike, these animals had the concentration of syndecan-1 two times higher compared to the controls (see the Table), a sign of glycocalyx degradation in the endothelial cells. The intensifying shedding of soluble syndecan-1 signifies the forming of the inflammatory endothelial cell phenotype and indicates that the adhesive properties and barrier functions are jeopardized [8-10]. Given that an increase in syndecan-1 was observed as early as on Day 7 after implanting non-biocompatible matrixes, measuring this marker in the blood can help predict scaffold non-vascularization.

On Day 7 after implanting polycaprolactone and vaterite matrices, the experimental white rats and the comparison rats alike had higher CRP concentrations than the controls. CRP levels normalized in the experimental group by Day 21. The CRP concentration change in the experimental group was no more significant than that in

the comparison group, meaning that such change was injury-induced. On Day 7 of implanting polycaprolactone and vaterite scaffolds, experimental animals had the VEGF concentration 3.1 times higher of the comparison rats, 1.6 times higher than that of the negative controls. By Day 21, VEGF concentration dropped in the experimental rats and did not differ significantly anymore from that of the controls, see the Table. Morphological methods earlier found that by Day 21, polycaprolactone and vaterite matrices were effectively vascularized [7]. Thus, a higher early post-implantation VEGF concentration gives a favorable scaffold vascularization prognosis.

Unlike the negative controls, the experimental rats did not have a significantly higher syndecan-1 concentration (see the Table), which showed the endotheliocyte glycocalyx did not sustain damage. The findings suggest that it is not a change in the VEGF concentration in blood, but the ratio of change in the VEGF and syndecan-1 concentrations in serum that is most valuable for predicting the angiogenic potential of scaffolds in subcutaneous implantation tests. Such predictions can be made biochemically as early as on Day 7 whereas literature data suggests [4] that the morphological evaluation of scaffold vascularization is only possible as early as on Day 14.

CONCLUSIONS

1. The complete normalization of CRP, VEGF, and soluble glycocalyx concentrations in sham-operated animals completely excludes surgery-associated tissue injury as a factor affecting the state of endothelial cells on Day 21 after implanting scaffolds.

2. Implanting non-biocompatible scaffolds triggers a pronounced systemic inflammatory response and prolonged activation of angiogenesis associated with glycocalyx degradation and an inflammatory endotheliocyte phenotype being formed.

3. Implanting polycaprolactone matrices triggers a systemic inflammatory response identical to that in sham-operated animals, meaning such matrices are biocompatible. A higher VEGF concentration early after implanting characterizes the high angiogenic potential of polycaprolactone and vaterite matrices provided there are no signs of damage to endothelial glycocalyx.

4. The angiogenic potential of scaffolds can be predicted from the endothelial cell state markers as early as on Day 7 before morphological signs of vascularization emerge. The ratio of change in the serum concentrations of VEGF and syndecan-1 is the most valuable marker for predicting the angiogenic potential of scaffolds in subcutaneous implantation tests.

FINANCIAL SUPPORT AND SPONSORSHIP

Nil.

CONFLICTS OF INTEREST

The authors declare no conflict of interest

REFERENCES

1. Bose S., Roy M., Bandyopadhyay A. Recent advances in bone tissue engineering scaffolds. *Trends in Biotechnology*. 2012, vol. 30, no. 10, pp. 546-554, doi 10.1016/j.tibtech.2012.07.005.

2. Perez R.A., Seo S.J., Won J.E. et al. Therapeutically relevant aspects in bone repair and regeneration. *Materials Today*. 2015, vol. 18, no. 10, pp. 573-589, doi 10.1016/j.mattod.2015.06.011.

3. Sharma S, Srivastava D, Grover S. et al. Biomaterials in tooth tissue engineering: a review. *Journal of Clinical and Diagnostic Research*, 2014, vol. 8, no. 1, pp. 309-315, doi 10.7860/JCDR/2014/7609.3937.

4. Ivanov A.N., Kozadaev M.N., Bogomolova N.V. et al. Biocompatibility of polycaprolactone and hydroxyapatite matrices in vivo. *Cell and Tissue Biology*. 2015, vol. 9, no. 5, pp. 422-429, doi 10.1134/S1990519X15050077.

5. Spiller K.L., Anfang R.R., Spiller K.J. et al. The role of macrophage phenotype in vascularization of tissue engineering scaffolds. *Biomaterials*. 2014, vol. 35, no. 15, pp. 4477-4488, doi 10.1016/j.biomaterials.2014.02.012.

6. Ivanov A.N., Saveleva M.S., Kozadaev M.N. et al. New Approaches to Scaffold Biocompatibility Assessment. *BioNanoScience*. 2019, vol. 9, no. 2, pp. 395-405, doi 10.1007/s12668-019-00613-3.

7. Saveleva M.S., Ivanov A.N., Kurtukova M.O. et al. Hybrid PCL/CaCO3 scaffolds with capabilities of carrying biologically active molecules: Synthesis, loading and in vivo applications. *Materials Science and Engineering: C*. 2018, vol. 85, pp. 57-67, doi 10.1016/j.msec.2017.12.019.

8. McDonald K.K., Cooper S., Danielzak L et al. Glycocalyx degradation induces a proinflammatory phenotype and increased leukocyte adhesion in cultured endothelial cells under flow. *PLoS One*. 2016, vol. 11, no. 12, p. e0167576, doi 10.1371/journal.pone.0167576.

9. Voyvodic P.L., Min D., Liu R. et al. Loss of syndecan-1 induces a pro-inflammatory phenotype in endothelial cells with a dysregulated response to atheroprotective flow. *Journal of Biological Chemistry*. 2014, vol. 289, no. 14, pp. 9547-9559, doi 10.1074/jbc.M113.541573.

10. Purushothaman A., Uyama T., Kobayashi F. et al. Heparanase-enhanced shedding of syndecan-1 by myeloma cells promotes endothelial invasion and angiogenesis. *Blood*. 2010, vol. 115, no. 12, pp. 2449-2457, doi 10.1182/blood-2009-07-234757

MOLECULAR AND MORPHOLOGICAL EFFECTS OF PROLONGED RADIOTHERAPY IN RECTAL CANCER

Novikova I.A., Dzhenkova E.A., Shaposhnikov A.V., Gusareva M.A., Kharagezov D.A., Duritskiy M.N., Dashkov A.V., Kolesnikov V.E., Snezhko A.V., Kaymakchi D.O., Mirzoyan E.A., Poluektov S.I., Dontsov V.A., Stateshny O.N.

Federal State Budgetary Institution «National medical research centre for oncology» of the Ministry of Health of the Russian Federation, Rostov-on-Don, e-mail: ellada-mirzoyan@yandex.ru

Aims

Study objective: to identify molecular and morphological effects of preoperative radiotherapy in rectal cancer.

Materials and Methods

We analysed data from 45 patients who underwent radiotherapy during the perioperative period. DNA (DNA distribution over the cell cycle phases) was tested in tumour cells of the resected intraoperative tumour tissue (CycleTESTTMPLUS DNA ReagentKit). The DNA index characterised by aneuploid to diploid cell ratio was determined. Therapeutic pathomorphism and change in tumour size induced by preoperative radiotherapy were recorded.

Results

The DNA index test has showed no tumours with DNA index less than 1.0. The index ranged from 1.1 to 1.9. Radiotherapy was associated with a 1.6-fold increase in tumour incidence with DNA index up to 1.5 and a 2.6-fold decrease in tumour incidence with DNA index greater than 1.5. Grade III therapeutic pathomorphism was reported in 70% of cases. The tumour extent decreased 1.5-fold, and the distance from the anus to the lower edge of the tumour increased 1.2-fold ($p<0.05$).

Conclusions

The molecular and morphological effect of radiotherapy for rectal cancer was a reduction in tumour malignancy potential, manifested by varying degrees of therapeutic pathomorphism. Our data suggest that, 6–8 weeks after prolonged radiotherapy, there is a pronounced clinicopathological effect, and the molecular changes already correspond to a non-irradiated tumour by many parameters at this time. Consequently, extending the period between the end of radiotherapy and surgery may result in resumption of tumour growth and reversal of the effect of neoadjuvant therapy. This should be considered when planning combination treatment in patients with rectal cancer.

Keywords: oncology, rectal cancer, radiotherapy, DNA.

INTRODUCTION

Modern oncology achieved significant success in the treatment of colorectal cancer [1–3] and radiotherapy was included in the combined therapy for colorectal cancer long ago [4, 5]. Numerous studies showed an important role of preoperational radiotherapy in a complex treatment for colorectal cancer. In the USA, from 2004 to 2011, the share of patients that received neoadjuvant radiotherapy increased from 57% to 75%, and the share of patients that received postoperative radiotherapy decreased from 39% to 18% [6, 7]. Similar tendencies were observed in Europe and Russia.

The indication of preoperational radiotherapy leads to a two-fold decrease in the 5-year rate of recurrence-free survival in patients with colorectal cancer (from 10.9% to 5.6%) [8–10]. It was established that the main prognostic sign of the effectiveness of radiotherapy in patients with malignant tumors was the degree of tumor regression. Thus, 3-year recurrence-free survival in patients with Dworak 4 is 95%, Dworak 3 – 82%, Dworak 2 – 64%, and Dworak 1 – only 53% [11]. The achievements in fundamental oncology allow specialists to evaluate the degree of tumor regression at the tissue, cellular, and molecular levels.

The study was aimed to reveal the molecular-morphological effects of perioperative radiotherapy in patients with colorectal cancer.

MATERIALS AND METHODS

The authors analyzed the data obtained from 45 patients with colorectal cancer T3-4N0-1M0 that underwent therapy at the National Medical Research Oncologi-

cal Center of the Ministry of Healthcare of the Russian Federation. In all the patients, the tumor was characterized as adenocarcinoma (more often, it was moderately differentiated (75%)). The main group included 20 patients that underwent a course of neoadjuvant radiotherapy for a tumor and pathways of metastases (19 sessions 5 times per week with a fraction dose of 2.4 Gy to a total boost dose of 50 isoGy). In the days of therapy, radiomodification with capecitabine (1600 mg2/day) was indicated. Surgical treatment was performed in 7–8 weeks after radiotherapy. The control group included 25 patients that had a contraindication to radiotherapy at the first stage or refused the therapy. A postoperational tumor specimen was sent for pathomorphological study. The degree of therapeutic pathomorphism of the tumor was identified by Lavnikova's method. Tissue DNA analysis was performed with the CycleTESTTMPLUS DNA ReagentKit (No. 340242, BectonDickinson). The obtained data were statistically processed with the ModFit LT software. The software was used to analyze the ploidy and distribution of cells by the phases of the cellular cycle. Besides, the share of cells with different content of DNA was calculated. The proliferation index was defined as the sum of tumor cells at the phase of S- and (G2+M) of the cellular cycle. Student's t-test was used for data processing.

The study protocol followed guidelines for experimental investigation with human subjects in accordance with the Declaration of Helsinki and was approved by the ethics committee. Written informed consent was obtained from each patient (or official representative) before the study.

RESULTS

The results of the morphological study showed that the changes in tumors after radiotherapy were characterized by the development of destructive foci. In the main group, the area of necrosis was 36.4±4.2%, the signs of irreversible forms of dystrophy varied from 24% to 68%. In the present study, therapeutic pathomorphism of grades I and IV was not revealed. Therapeutic pathomorphism of grade II was revealed in 25% of patients and grade III – in 70% of patients. It manifested itself as the lack of tumor cells, expressed fibrosis and hyalinosis of the connective tissue, the presence of focal calcification, and gigantic multinucleate cells like foreign matter. Flow cytometry was used to study the quantity of DNAs in tumor cells, their distribution by the phases of the cellular cycle, and proliferative activity of tumor cells under the influence of a course of neoadjuvant radiotherapy. It was proved that the content of DNA in a normal cell was inconstant. It is also known that a tumor is heterogeneous. The tumor growth is provided by an actively proliferating cell fraction. The cells at the phase of synthesis (S) and pre-synthesis (G1) are least sensitive to a radiative effect and cells at the phase of mitosis (M) and pre-mitosis (G2) are most sensitive.

The effect of drugs was different. Some alkylating agents affect the cells in the synthetic and pre-mitosis phase; plant-derived cytostatics – at the phase of mitosis, inhibitors of protein synthesis – in the pre-synthetic phase; and the effect of antimetabolites is observed in the synthetic and pre-synthetic phases. The study of DNA-cytometric parameters of colorectal tumors under the influence of radiotherapy revealed the prevalence of aneuploid tumors (60%) over diploid ones (40%). The share of tumors with a DNA index higher than 1.5 was 16.7%. In the control group, the share of aneuploid tumors was 64%. The majority of tumors were heterogeneous, i.e. they contained both aneuploid and diploid cells. The main factor that defines the biological behavior of the tumor is the characteristics of the mean content of aneuploid cells in the tumor. The performed analysis did not reveal any significant differences in the content of aneuploid cells in the tumor (51.9±4.7% and 51.4±5.3%, respectively). Aneuploidy is associated not only with the changes in DNA content in cells but also with the changes in the genome. It is characterized by the DNA index, which is the ratio of the intensity of the fluorescence peak of aneuploid to diploid cells. The results of the analysis of the indices in the groups showed that there were no tumors with the DNA index < 1.0; the DNA index varied from 1.1 to 1.9.

The mean value in the control group was 1.5±0.08, and in the main group, it was – 1.2±0.07. Besides, in the main group, tumors with the DNA index > 1.5 were identified only in 16.7% of cases ($p<0.05$).

Table 1

Distribution of cells by the phases of the cellular cycle (%)

Groups	G0/G1-phase	G2+M	S-phase
Main group	86.2±3.7	2.7±0.6	11.2±3.2
Control group	87.96±2.18	2.12±0.4	9.98±1.6

Table 2

The ratio of cells by the phases of the cellular cycle of diploid and aneuploid colon tumors (%)

Tumor type	G0/G1-phase	G2+M-phase	S-phase	Proliferation index
Diploid	86.3±4.3	0.11±0.008 ↓*	13.7±4.3	14.4±3.4
Aneuploid	86.2±5	3.5±0.9	10.4±2.1	13.9±3.4

N o t e : * – differences in the parameters were significant concerning aneuploid tumors ($p \leq 0.05$).

Table 1 shows the distribution of tumor cells depending on the phase of the cellular cycle. It was established that in the main group, a significant share of tumor cells was at the phase of G0/1 of the cellular cycle (86.2±3.7%) and the phase G2+M – 2.7±0.6%. The rate of cell proliferation was 11.2±3.2%, while the proliferative activity was 13.5±3.2%. In the control group, a similar distribution was observed: most of the cells were at the phase G0/1 – 87.96±2.18%, at the S-phase – 9.98±1.6%, and at G2+M phase – 2.12±0.4%.

The analysis of proliferative activity revealed similar index values in both groups of patients: 13.5±3.2% and 12.1±1.4%, respectively. The authors also analyzed the ratio between diploid and aneuploid tumor cells (Table 2).

Patients with diploid and aneuploid colorectal tumors are characterized by the prevalence of cells at the phase G0/1 of the cellular cycle. The authors revealed significant differences in diploid and aneuploid tumors ($p \leq 0.05$): the share of cells in the M and G2 phases was 32 times lower in diploid tumors.

The rate of proliferation in diploid cells exceeded the same parameter in aneuploid cells.

The indices of the proliferation of diploid and aneuploid tumors were similar.

Figs. 1–4 show histograms of the ratio of tumor cells in the studied groups.

Taking into account the fact that the main aim of preoperational radiotherapy in patients with colorectal cancer is a decrease in the primary tumor, the authors also evaluated the clinical effectiveness of the performed radiotherapy (Table 3).

It was revealed that in the group of patients that underwent prolonged radiotherapy, the tumor reduced from 6.8±0.6 cm to 4.5±0.5 cm ($p<0.05$), and the distance from the anus to the lower border of the tumor increased from 6.3±0.6 cm to 7.6±0.6 cm ($p<0.05$).

The authors revealed a clinical-morphological effect of pre-operational prolonged radiotherapy in patients with colorectal cancer. Thus, the clinical effectiveness of the therapy manifested itself as a decrease in the colorectal tumor length by 1.5 times and an increase in the distance between the anus and the lower border of the tumor by 1.2 times ($p<0.05$). Morphologically, these data were confirmed by the development of therapeutic pathomorphism of grade III in 70% of patients. The study at the molecular level revealed significant changes in the content of DNA in tumor cells of the rectum after radiotherapy. A prevalence of tumors with the DNA index < 1.5 by 1.5 times and a decrease in tumors with the DNA index >1.5 by 2.6 times in the main group of patients were observed. Besides, there was a significant decrease in the DNA index from 1.5±0.08 in the control group to 1.2±0.07 in the main group ($p \leq 0.05$).

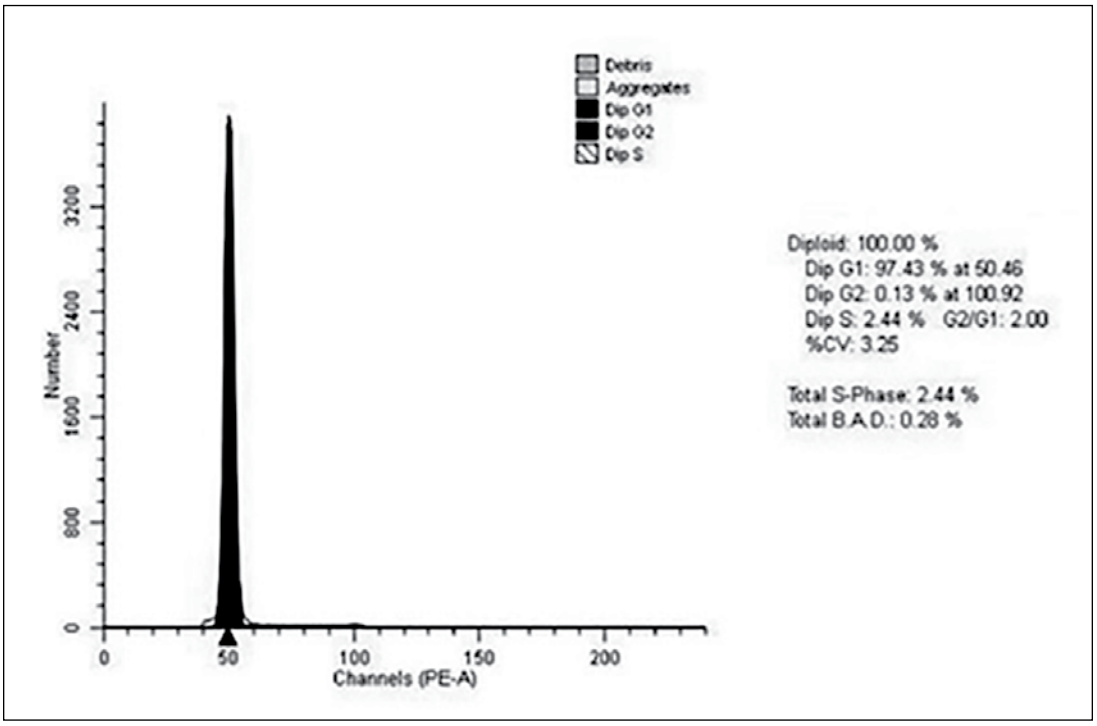

Fig. 1. Histogram of the distribution of cells by the phases of the cellular cycle of a diploid colorectal tumor in the main group. Patient M., female, 62 years old, histologically – G2 adenocarcinoma

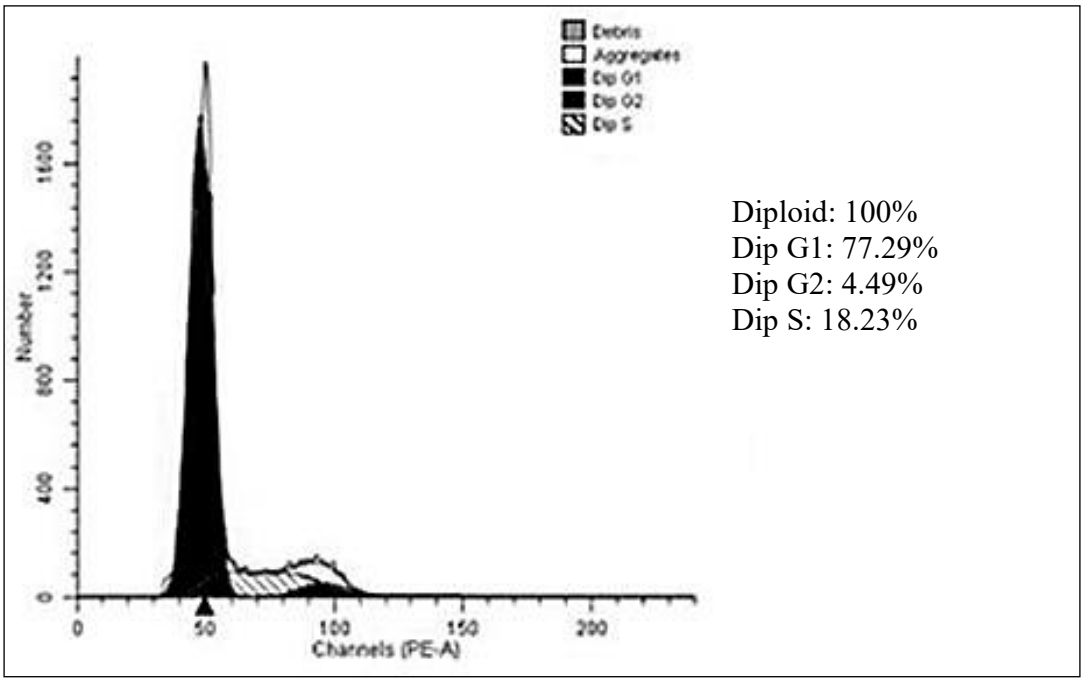

Fig. 2. Histogram of the distribution of cells by the phases of the cellular cycle of a diploid rectal tumor in the control group. Patient M., male, 61 years old, histologically – G2 adenocarcinoma

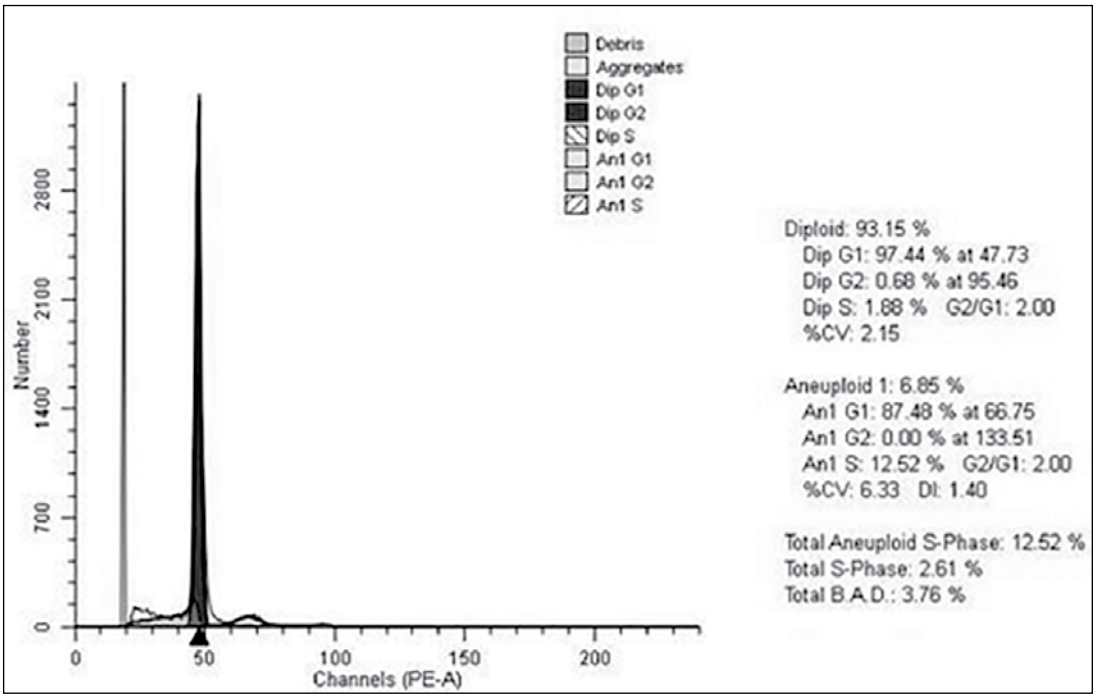

Fig. 3. Histogram of the distribution of cells of an aneuploid rectal tumor in the main group by the phases of the cellular cycle. Patient K., male, 55 years old, histologically – G2 adenocarcinoma

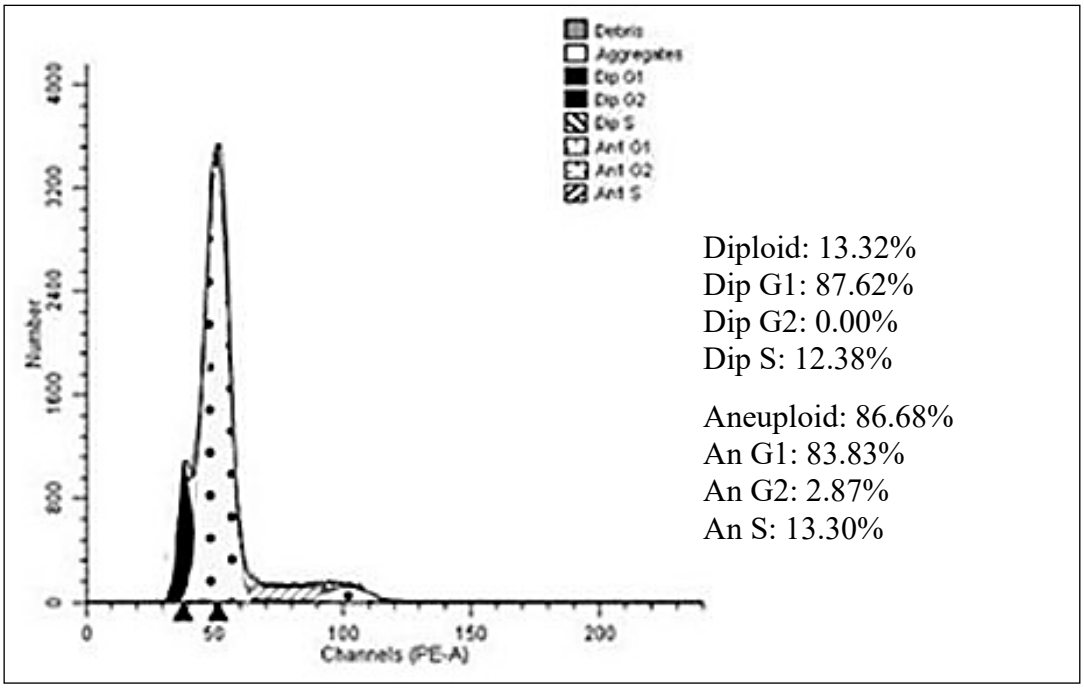

Fig. 4. Histogram of the distribution of cells of an aneuploid rectal tumor in the control group by the phases of the cellular cycle. Patient Sh., female, 47 years old, histologically – G2 adenocarcinoma

Table 3

Characteristics of rectal tumor after a course of radiotherapy

Characteristics of the tumor	Main group	Control group
Tumor length: before after	 6.8±0.6 cm 4.5±0.5 cm*	6.0±0.9 cm
Distance from the anus to the tumor: before after	 6.3±0.6 cm 7.6±0.6 cm 5856*	7.8±0.8 cm

N o t e : * – differences in the group are significant ($p<0.05$).

There were no significant changes revealed in the share of cells at different stages of the cellular cycle in tumors from the main and control groups. Still, radiotherapy led to significant differences between diploid and aneuploid tumors by the share of cells at the stage of mitosis (M) and premitosis (G2) of the cellular cycle that was 32 times lower in diploid than aneuploid tumors ($p\leq0.05$). Pre-operational radiotherapy in patients with colorectal cancer did not reveal significant differences in the share of aneuploid tumors and the mean content of aneuploid cells in the tumor in comparison with the control group. Aneuploid tumors were characterized by the lack of tumors with the DNA index < 1.0 in the main and control groups. The obtained data indicate that 6–8 weeks after prolonged radiotherapy, an expressed clinical morphological effect is observed and the changes at the molecular level at this period correspond to the parameters of a non-irradiated tumor. Thus, an excessive period between the end of the radiotherapy course and surgical intervention can lead to a recurrence of the tumor growth and ineffective neoadjuvant therapy. This fact should be accounted for when planning combined therapy in patients with colorectal cancer.

CONCLUSIONS

1. A decrease in the potential malignancy of colorectal cancer became the main molecular-morphological effect of preoperational radiotherapy. It was observed in the therapeutic pathomorphism of grade III (70%) and an increase in the rate of tumors with the DNA index up to 1.5 by 1.5 times.

2. The clinical effectiveness of preoperational radiotherapy is expressed as a decrease in the length of a colorectal tumor by 1.5 times and an increase in the distance from the anus to the lower border of the tumor by 1.2 times ($p<0.05$).

FINANCIAL SUPPORT AND SPONSORSHIP
Nil.

CONFLICTS OF INTEREST
The authors declare no conflict of interest

REFERENCES

1. Kit O.I., Gevorkian Iu.A., Soldatkina N.V. et al. Combined surgery for locally advanced colorectal cancer [Kombinirovannye operativnye vmeshatel'stva pri mestno- rasprostranennom kolorektal'nom rake]. *Pirogov Russian Journal of Surgery - Khirurgiia. Zhurnal imeni N.I. Pirogova*, 2016, no. 11, pp. 42-47, doi: 10.17116/hirurgia20161142-47.

2. Kit O.I., Vodolazhskiy D.I., Gevorkyan Y.A. et al KRAS Gene Mutations and Gender Differences in Colorectal Cancer. *International Journal of Bio Medicine*. 2015, vol. 5, no.1, pp.11-15, doi 10.21103/Article5(1)_CR2.

3. Kit O.I., Gevorkian Iu.A., Soldatkina N.V. et al. Frequency and spectrum of kras gene mutations in advanced colorectal cancer. Clinical-morphological features [Chastota i spektr mutatsii gena KRAS pri rasprostranennom kolorektal'nom rake]. *Molecular medicine - Molekuliarnaia meditsina*, 2015, no. 5, pp. 26-29.

4. Ferrari L. Neoadjuvant chemoradiation therapy and pathological complete response in rectal cancer. *Gastroenterol Rep (Oxf)*. 2015, vol. 3, no.4, pp. 277-288.

5. Abrams M.J., Koffer P.P., Leonard K.L. et al. The emerging non-operative management of non-metastatic rectal cancer: A population analysis. *Anticancer Research*. 2016, vol. 36, no. 4, pp. 1699-1702.

6. Gahagan J.V., Whealon M.D., Phelan M.J. et al. Improved survival with adjuvant chemotherapy in locally advanced rectal cancer patients treated with preoperative chemoradiation regardless of pathologic response. *Surgical Oncology*. 2020, vol. 32, pp. 35-40, doi 10.1016/j.suronc.2019.10.021

7. Kreis M.E., Ruppert R., Kube R. et al. MRI-Based Use of Neoadjuvant Chemoradiotherapy in Rectal Carcinoma: Surgical Quality and Histopathological Outcome of the OCUM Trial. *Annals of Surgical Oncology*. 2020, vol. 27, no. 2, pp. 417-427, doi 10.1245/s10434-019-07696-y.

8. Maas M., Dijkhoff R.A.P., Beets-Tan R., Rectal Cancer: Assessing Response to Neoadjuvant Therapy. *Magnetic Resonance Imaging Clinics of North America*. 2020, vol. 28, pp.117-126.

9. Maeda K., Shibutani M., Tachimori A. et al. Prognostic significance of neoadjuvant rectal score and indication for postoperative adjuvant therapy in rectal cancer patients after neoadjuvant chemoradiotherapy. *In Vivo*. 2020, vol. 34, no. 1, pp. 283-289, doi 10.21873/invivo.11772.

10. Taylor F.G., Quirke P., Heald R.J. et al. Preoperative magnetic resonance imaging of circumferential resection margin predicts disease-free survival and local recurrence: 5-year follow-up results of the MERCURY study. *Journal of Clinical Oncology*. 2014, vol. 32, no. 1, pp. 34-43, doi 10.1200/jco.2012.45.3258.

11. McCoy M.J. Neoadjuvant chemoradiotherapy for rectal cancer: how important is tumor regression? *ANZ Journal of Surgery,* 2015, vol. 5, pp. 23-29.

FEATURES OF SURGICAL CORRECTION OF CONGENITAL SMALL BOWEL OBSTRUCTION: CLINICAL EXPERIMENTAL STUDY

Zheleznov A.S.[1], Ermolaeva N.S.[1], Otdelnov L.A.[1], Senina M.S.[1,2]

[1]Privolzhsky Research Medical University of Ministry of Health of Russia, Nizhny Novgorod, e-mail: rector@pimunn.ru;

[2]The Ministry of Health of the Nizhny Novgorod region, Nizhny Novgorod, e-mail: official@zdrav.kreml.nnov.ru

Aims

Study objective: to determine the structure of the congenital bowel obstruction, and to evaluate the efficacy and safety of various methods for its surgical correction.

Materials and Methods

A retrospective analysis of 45 case records of children with congenital bowel obstruction was carried out. The following surgeries were performed for jejunoileal obstruction: adapted anastomosis, end-to-side small-large bowel anastomosis, plication anastomosis per de Lorimier-Harrison, and in the case of multiple small bowel atresia, the end-to-end and T-shaped anastomoses were performed using the Bishop-Koop technique, and ileo- and jejunostomy was carried out. The following was carried out for duodenal obstruction: duodenoduodenal anastomosis using Kimura's technique, side-to-side anastomosis, end-to-side anastomosis, duodenotomy with membrane excision, Ladd procedure and duodenoileostomy. During the experimental phase, 10 small-small bowel anastomoses per de Lorimier-Harrison were done in rabbits with interrupted (n=5) and continuous (n=5) suture, followed by evaluation of their elasticity and tightness.

Results

The following complications of duodenal atresia were reported: functional anastomotic leak (n=1), adhesive-obturative obstruction (n=1). The following was reported in the case of jejunoileal atresia correction: functional anastomotic leak (n=1), adhesive-obturative obstruction (n=1), and one case of combination of these complications. Based on experimental results, the continuous intestinal suture was found to be safer than the interrupted one in the plication anastomosis. The adaptive anastomoses give better results in jejunoileal obstruction. In 4:1 discongruence of small intestinal segments, the plication anastomosis is optimal; duodenoduodenal anastomosis using Kimura's technique is the method of choice for the treatment of duodenal obstruction.

Conclusions

The use of a one-row contiguous suture in plication anastomosis increases the elasticity and tightness of the anastomotic zone, is less traumatic, and, therefore, can be recommended in the surgical treatment of children with congenital bowel obstruction.

Keywords: neonatal surgery, congenital bowel obstruction, entero-entero anastomosis, jejunoileal atresia, duodenal atresia.

INTRODUCTION

According to the WHO, annually, 5–6% of children are born with congenital anomalies, more than 300,000 of them die within the first four weeks after birth. In Russia, congenital anomalies rank second among early neonatal death causes (18.1%) [1]. In their structure, anomalies of the gastrointestinal tract occupy second place leaving the first one to heart defects. The most frequent cause of congenital intestinal obstruction is atresia. Atresia is primarily localized in the areas of "complicated" organogenesis: esophagus, duodenum, distal ileum, and ileocecal junction [2, 3]. The rate of occurrence of intestinal atresia is 1:5,000 newborns [4]. Patients with atresia of the jejunum have an increased risk of the development of a short bowel syndrome [5].

A diversity of pathomorphological variants of intestinal defects determines difficulties in the choice of surgical tactics for a certain pathology and the technique of anastomosis formation [6]. Presently, pediatric surgeons do not have a consistent opinion on the choice of methods of surgical correction of congenital intestinal obstruction.

The study was aimed to identify the structure of congenital intestinal obstruction, to evaluate the efficiency and safety of different methods of its surgical correction.

MATERIALS AND METHODS

The authors performed a retrospective analysis of 45 medical histories of children hospitalized to the surgical department of Nizhny Novgorod Regional Clinical Hospital for Children from 2011 to 2017 with congenital intestinal obstruction. The study included 21 patients (47%) with high intestinal obstruction (13 females and 8 males) and 24 patients (53%) with low intestinal obstruction (8 females and 16 males).

The etiology of congenital intestinal obstruction is presented in Figures 1 and 2.

All patients underwent surgery. Ten patients (22%) had Kimura duodenoduodenal anastomosis formed; 3 children (6.6%) underwent duodenotomy with a membrane dissection; in 4 cases (4.4%), end-to-side (n=2) and side-to-side (n=2) anastomoses were formed; and in 2 cases (6.6%), children with Ladd's syndrome underwent Ladd's surgery. One child with a combination of duodenal stenosis and Ladd's syndrome underwent dissection of Ladd's bands and duodenoileostomy.

Seven patients (15.5%) with jejunoileal atresia had adapted anastomosis formed; 5 patients (11%) had end-to-side anastomosis formed.

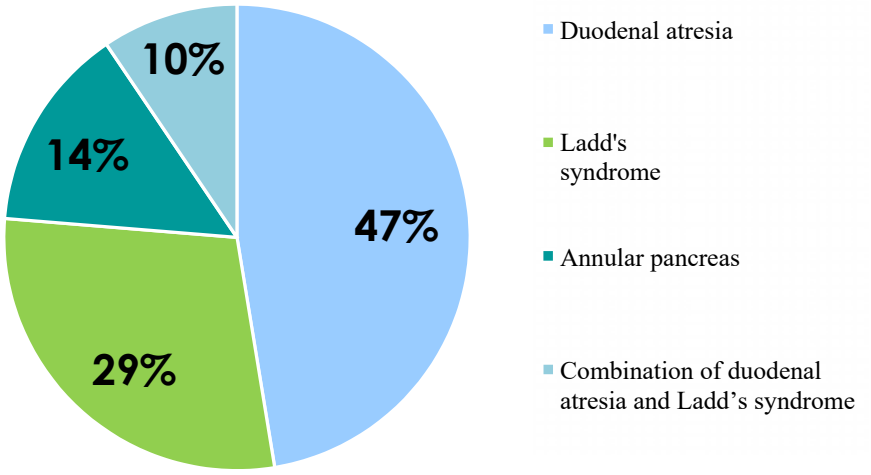

Fig. 1. Distribution of patients with high congenital intestinal obstruction by the etiology

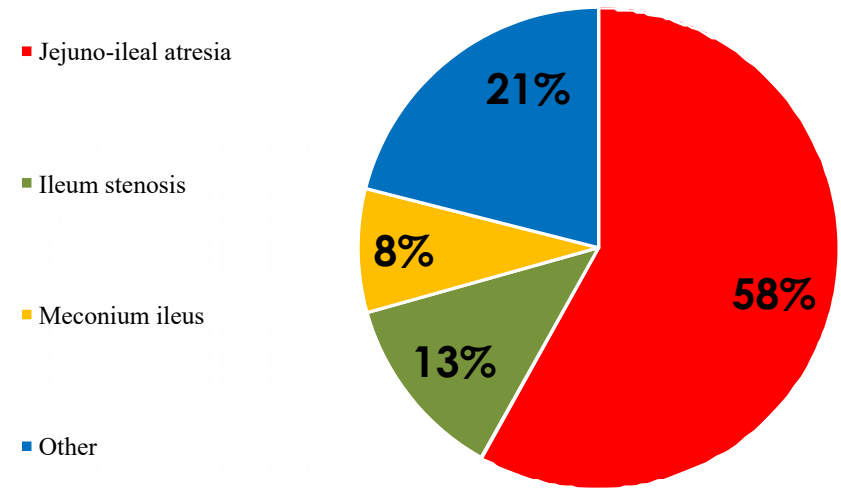

Fig. 2. Distribution of patients with low congenital intestinal obstruction by the etiology

Fig. 3. Anastomosis leakage check by the method of pneumopression

Four patients (8.9%) underwent ileostomy (n=2 in patients with meconium ileus, n=2 in patients with ileal stenosis). One patient (2.2%) underwent jejunostomy. One child with a "pagoda" syndrome had de Lorimier–Harrison plication anastomosis formed. In cases with multiple intestinal atresias, end-to-end and T-shaped Bishop–Koop anastomoses were performed (2.2%).

During the experimental part of the study, the authors performed de Lorimier–Harrison ileoileal plication anastomoses to 10 male brush rabbits (n=5 – loop sutures, n=5 – continuous suture). The mean duration of the surgery was 103 + 24.9 minutes. Rabbits were narcotized with nembutal, zoletil, and novocaine. Preoperative antibiotic prophylaxis and antibiotic treatment (gentamycin) were performed for 3 days. Infusion therapy (5% solution of glucose, mexidol, 40–50 ml) was performed during the surgery. Animals were withdrawn from the experiment on Day 7 using the method of air embolism.

The study was performed according to the European Convention for the Protection of Vertebrate Animals Used for Experimental and Other Scientific Purposes (Strasburg, March 18, 1986, ETS No. 123). The study was approved by the local ethical committee.

The morphological study was performed using a microscope Nikon Eclipse 80 I, 10×22. Anastomosis leakage was detected by the method of pneumopression. The anastomosis area was identified. An air feeding tube was fixed to the distal end. The proximal end had a manometer attached. The pressure required for anastomosis leakage was registered (Figure 3). For the evaluation of elasticity of anastomosis, the index of stenosing (IS) was calculated by the following formula (Irvin, 1977):

$$IS = 100 \cdot (1 - 2 \cdot \frac{A}{B + C}) (\%),$$

where A is the diameter of the bowel in the area of the anastomosis, B is the diameter of the bowel 2 cm higher than the anastomosis, and C is the diameter of the bowel 2 cm lower than the anastomosis.

Statistical analysis included methods of descriptive statistics with the calculations for the samplings of such parameters as arithmetical mean, median, the error of the arithmetical mean, and mean-square deviation. The significance of parametric data was evaluated using Student's t-test and non-parametric data – Mann-Whitney U-test. The results were significant at $p<0.05$. The obtained values were rounded to the second decimal.

The study protocol followed guidelines for experimental investigation with human subjects in accordance with the Declaration of Helsinki and was approved by the ethics committee. Written informed consent was obtained from each patient (or official representative) before the study.

RESULTS

Among 10 operated rabbits that underwent Kimora's duodenoduodenal anastomosing, 1 developed a complication expressed as functional anastomosis leakage. In 1 case, adhesive obstruction developed in the side-to-side anastomosis.

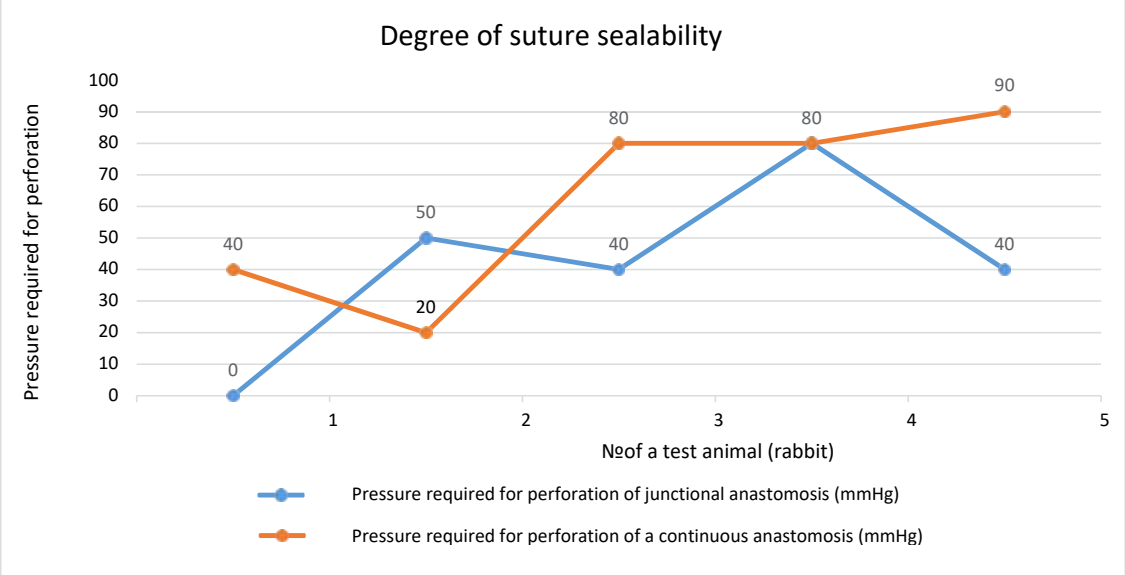

Fig. 4. A comparative evaluation of the suture sealability of junctional and continuous anastomoses

Results of the evaluation of the degree of suture sealability (junctional/continuous)

	The pressure required for leakage (junctional anastomosis), mm Hg	The pressure required for leakage (continuous anastomosis), mm Hg
Mean	42	56
Median	40	60
Observations	5	5
Hypothetical mean difference	0	0
P (T<=t) one-tailed	0.0418	

After the correction of jejunoileal atresia by the method of adaptive anastomosing (n=7), 1 rabbit developed functional anastomosis leakage. End-to-side anastomosing led to 2 complications: adhesive obstruction and a combination of anastomosis leakage and adhesive obstruction.

The experimental part showed that in cases of forming de Lorimier-Harrison plication anastomosis, one-row continuous suturing had the best statistical results by the parameters of elasticity and sealability of the anastomosis (Figure 4, Table 1).

Figure 4 and Table 1 show that loop suturing was perforated in the area of anastomosis at a significantly lower pressure than continuous suturing. The mean pressure required for anastomosis leakage formed with loop suturing was 42 mm Hg, while in cases with continuous suturing, it was 56 mm Hg ($p<0.05$).

The evaluation of elasticity of anastomosis by the calculation of stenosing indices on Day 7 showed that in cases of continuous suturing, it was 15.2%+/–2.4%, and loop suturing – 19.1%+/–2.4%, which indicates that loop suturing is more rigid and the continuous suturing is more elastic.

The morphological study of the area of anastomosis revealed that loop suturing results in a complete lack of intestinal villi, foci of hemorrhage, necrotized masses on the surface (cellular detritus), hydropic degeneration, as well as significantly damaged epithelium and intermuscular nervous plexuses (Figures 5, 6).

In cases of continuous suturing, specific epithelium villi, goblet cells, functioning crypts, blood filling, and nervous ganglia were preserved, which indicates a lower traumatizing capacity of this suture (Figures 7, 8).

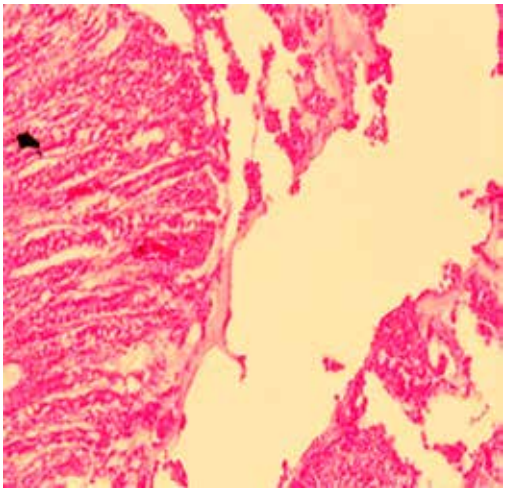

Figure 5. Histological picture of the area of anastomosis made by loop suturing (lack of intestinal villi, foci of hemorrhage)

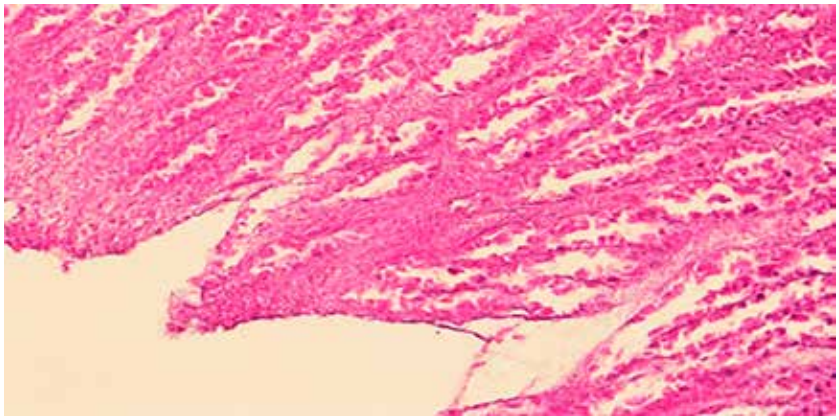

Figure 6. Histological picture of the area of anastomosis made by loop suturing (completely damaged epithelium)

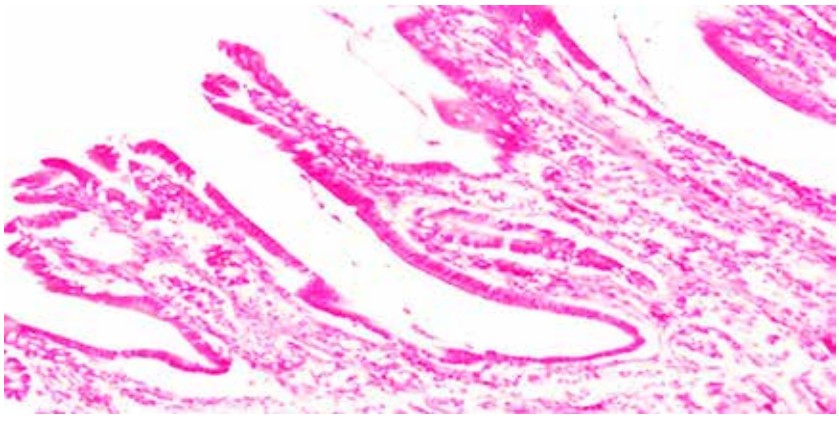

Figure 7. Histological picture of the area of anastomosis made with continuous suturing (villi with specifically preserved epithelium, goblet cells)

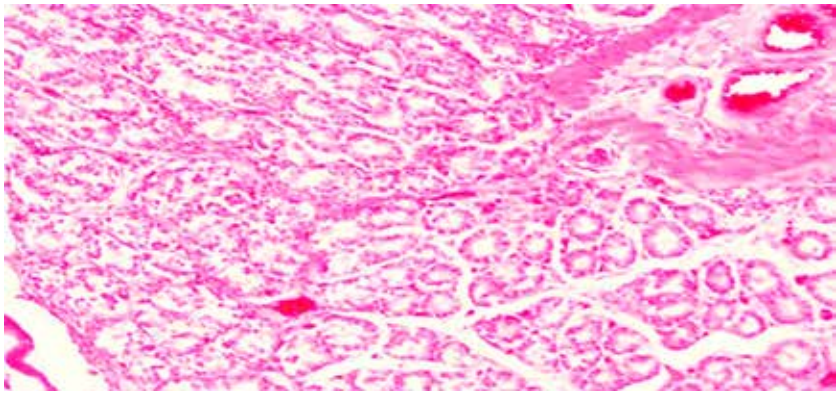

Figure 8. Histological picture of the area of anastomosis made with continuous suturing (blood filling was preserved)

CONCLUSIONS

The issue of the approaches to surgical correction for congenital intestinal obstruction remains open due to the lack of unified tactics for the treatment of this pathology. The effectiveness of the methods of surgical correction of the specified pathologies requires further study in the area of evidence-based medicine and larger samplings. The present study showed that the method of choice in the treatment for duodenal obstruction could be Kimura's duodenoduodenal anastomosis, for a membranous type of atresia – dissection of the membrane, for jejunoileal obstruction – adaptive anastomosis, for discongruence of the intestinal segments > 4:1 – plicate anastomosis, which morphological characteristics are underdescribed in the published literature. The application of one-row continuous suture when forming plicate anastomosis increases the elasticity and scalability of the area of anastomosis and is less traumatizing. Thus, it can be recommended for the surgical treatment of children with congenital intestinal obstruction.

CONFLICTS OF INTEREST

The authors declare no conflict of interest

REFERENCES

1. Shchegolev A.I., Pavlov K.A., Dubova E.A. et al. Early neonatal mortality in the Russian Federation in 2010 [Ranniaia neonatal'naia smertnost' v Rossiiskoi Federatsii v 2010 g.]. *Archive of Pathology - Arkhiv patologii*, 2013, no. 1, pp. 15-19.

2. Botvin'ev O.K., Eremeeva A.V., Kondrikova E.V. Duodenal atresia in the newborn [Atreziia dvenadtsatiperstnoi kishki u novorozhdennykh]. *Archive of Pathology - Arkhiv patologii.* 2012, no 5, pp. 32-35.

3. Petrenko V.M. Embryonic foundations of human congenital duodenal obstruction [Embrional'nye osnovy vozniknoveniia vrozhdennoi neprokhodimosti dvenadtsatiperstnoi kishki cheloveka]. *International Journal of Experimental Education - Mezhdunarodnyi zhurnal eksperimental'nogo obrazovaniia* , 2017, no. 2, pp. 56-57.

4. Lima M., Ruggeri G. Evolution of the surgical management of bowel atresia in newborn: laparoscopically assisted treatment. *Pediatr Med Chir*. 2009, vol. 3, no. 5, pp. 215-219.

5. Dao D.T., Demehri F.R., Barnewolt C.E. et al. A new variant of type III jejunoileal atresia. *Journal of Pediatric Surgery*. 2019, vol. 54, no. 6, pp. 1257-1260, 10.1016/j.jpedsurg.2019.02.003.

6. Savvina V.A. Varfolomeev A.R. Okhlopkov M.E. Congenital intestinal obstruction: choice of surgical tactics and intestinal suture technique [Vrozhdennaia kishechnaia neprokhodimost': vybor khirurgicheskoi taktiki i tekhniki kishechnogo shva]. - *Russian Herald - Rossiiskii vestnik*, 2012, vol. 2, no. 2, pp. 69-73.

ASSESSMENT OF THE STATE OF VERTEBROPELVIC RELATIONS IN CHILDREN WITH BILATERAL HIGH-STANDING GREATER TROCHANTER

Bortulev P.I.[1], Vissarionov S.V.[1,2], Baskov V.E.[1], Pozdnikin I.Yu.[1], Barsukov D.B.[1]

[1]The Turner scientific research institute for children's orthopedics, St. Petersburg, Pushkin, e-mail: pavel.bortulev@yandex.ru;

[2]Mechnikov North-Western State Medical University, St. Petersburg

Aims

The aim of the study was to investigate the parameters of sagittal vertebropelvic relations and to determine the type of vertical posture in children with bilateral high-standing greater trochanter.

Materials and Methods

The study included 30 patients (60 hip joints) aged 13 to 16 years (14.5 ± 0.9) with bilateral high-standing greater trochanter. All patients underwent routine orthopaedic examination with Harris Hip Score and Oswestry [sic: Oswestry Disability Index]. All patients underwent X-ray measurements of the parameters characterising the state of the hip joint and sagittal vertebropelvic relations.

Results

Clinical and radiological changes in the sagittal vertebropelvic relations manifest as hyperlordosis of the lumbar spine, which results from excessive pelvic anteversion. A strong positive correlation was found between the height of the greater trochanter and the slope of the sacrum – the Pearson coefficient was 0.69. Children with high-standing greater trochanter have a marked increase in global lumbar lordosis (GLL), sacral slope (SS), decrease in pelvic tilt (PT), and displacement of the sagittal vertical axis (SVA) posterior to the sacral promontory. This type of X-ray picture corresponds to the IV (hyperlordotic) type of vertical posture according to P. Roussouly.

Conclusions

The childhood anatomic changes in the hip joints are a substrate for the development of extra-articular type of femoracetabular impingement and early coxarthrosis, and compensatory changes in the lumbosacral spine predetermine the formation of mechanisms for early development of degenerative dystrophic processes.

Keywords: high-standing greater trochanter, sagittal vertebropelvic relations, excessive pelvic anteversion, hyperlordosis.

INTRODUCTION

Hip diseases are associated with the deformities of hip components. There are nosological forms where the hip sustains a multiplane deformity, and the greater trochanter becomes high-riding. These diseases include the sequelae of acute hematogenous osteomyelitis, Perthes disease, juvenile epiphysiolysis of the femoral head, congenital and acquired varus deformities of the femoral neck. Besides, some researchers report that a high-riding greater trochanter can be a result of the suffered post-immobilization ischemic necrosis of the femoral head after a single femoral head reduction followed by rigid immobilization of the lower limbs as part of treating hip dysplasia, or after hyperbaric oxygenation is applied to a neonate, which affects the growth plates [1; 2].

Murray (1965) was the first to suggest that coxarthrosis might be connected to the anatomical change in the proximal femur. This condition was further named femoroacetabular impingement, the pathomechanics of which was detailed by Leunig and Ganz [3; 4]. Further research of this pathology identified several types of extraarticular femoroacetabular impingement, with trochanteric-pelvic impingement being the most common type [5; 6]. A high-riding trochanter that has emerged in a child will further limit the amplitude of hip movement, resulting in lameness and a progressive weakness of the gluteal muscles. Besides, a long-lasting high-riding trochanter might in some patients lead to a hip subluxation, which in turn results in pain and early coxarthrosis.

It is well-known that any change in the kinetic system comprising the hip joints and the lumbar spine may lead to anatomical and biomechanical change in the joints and in the spinal motion segments alike. Besides,

the system is capable of self-overburdening, which has been described in detail for children with various spine pathologies and dysplastic hip subluxation, as well as for adults suffering from hip-spine syndrome.

High-riding greater trochanter is mainly treated surgically. Appropriate anatomical ratios are attained by corrective osteotomy of the femur or reducing the greater trochanter and resecting the femoral head; sometimes, all these methods are combined [9; 10].

However, the scientific literature available today has no data on the state of the sagittal spine-hip ratios that would determine the type of vertical posture in children suffering bilateral high-riding greater trochanter.

The goal hereof was to study the sagittal spine-hip ratios and to determine the vertical posture type in children suffering bilateral high-riding greater trochanter.

MATERIALS AND METHODS

This research involved 30 patients (60 hip joints) aged 13 to 16 (14.5 ± 0.9), all with a bilateral high-riding greater trochanter. Eighteen patients were female (60%) and 12 were male (40%). The inclusion criteria were: the age, the Risser Grade above 3, the apex of the greater trochanter being above the center of rotation of the femoral head with a shorter neck, destabilization of the hip, no femoral head deformity, no flexion contracture in the hip joints, no congenital or acquired spinal pathology, no neurological disorders, no systemic or genetic pathology, no spinal or hip surgery in the history.

The exclusion criteria were: hip subluxation or dislocation, surgical iatrogenic etiology of deformities, varus deformity of the proximal femur (neck-shaft angle <115°), and genetically verified systemic skeletal dysplasia.

Clinical examination was carried out following the standard methodology for patients with hip pathologies (Marx, 1978). To collect the most objective data on the patients' complaints, the research team used the Harris hip score and Oswestry questionnaires. Pain syndrome severity was measured on the international visual analog scale (VAS). Radiological examination methods included hip X-ray (antero-posterior view and Lauenstein projection), as well as lateral panoramic X-ray of the spine (C1 to S1) also covering the femurs, taken off a standing patient. Radiological examination was used to calculate the Sharp and Wiberg angles, the extent of hip impingement, the neck-shaft angle, the proximal femur anteversion angle, the trochanter-to-trochanter distance (TTD), the center-trochanter distance (CTD), the thoracic kyphosis (TK) and global lumbar lordosis (GLL) degree, the pelvic incidence (PI), the sacral slope (SS), the pelvic tilt (PT), and the sagittal vertical axis (SVA).

X-ray data was evaluated in Surgimap v. 2.2.15.5. Statistical analysis was run in Excel 2010 and IBM SPSS Statistic v.23 (USA). As part of the analysis, the researchers calculated the means and the standard deviation for each indicator. Pearson's test was used for correlation analysis.

The research was discussed and approved by the Ethics Committee of H. Turner National Medical Research Center for Children's Orthopedics and Trauma Surgery (the Turner Center). The patients and their representatives consented to participation and publication of their personal data.

RESULTS

Upon admission to the Hip Unit of the Turner Center, 23 patients (76.7%) complained of bad gait, limited hip abduction, and pain syndrome, mainly on the posteriolateral femoral surface, experienced after walking continuously for 2 hours or after minor physical activity; they also complained about pain in the lumbar spine. Other patients (7, 23.3%) complained mainly about lameness and hip joint dysfunction. Pain syndrome in the lumbar spine would only be produced by exercising. The Harris hip score and Oswestry questionnaires returned 66.6±4.7 points and 21.5±3.7%, respectively. This suggested restrictions in the lifestyle characteristic of this age category due to hip dysfunction and pain in the lumbar spine. History analysis shed light onto what caused bilateral high-standing greater trochanter, see Figure 1.

Twenty-three patients (76.7%) developed the condition from acute hematogenous osteomyelitis survived as a neonate; 5 patients (16.7%) had it due to treatment of hip dysplasia of varying severity by Lorenz's method, and 2 patients (6.6%) had a hypertrophic greater trochanter due to extracorporeal membrane oxygenation they had experienced as neonates.

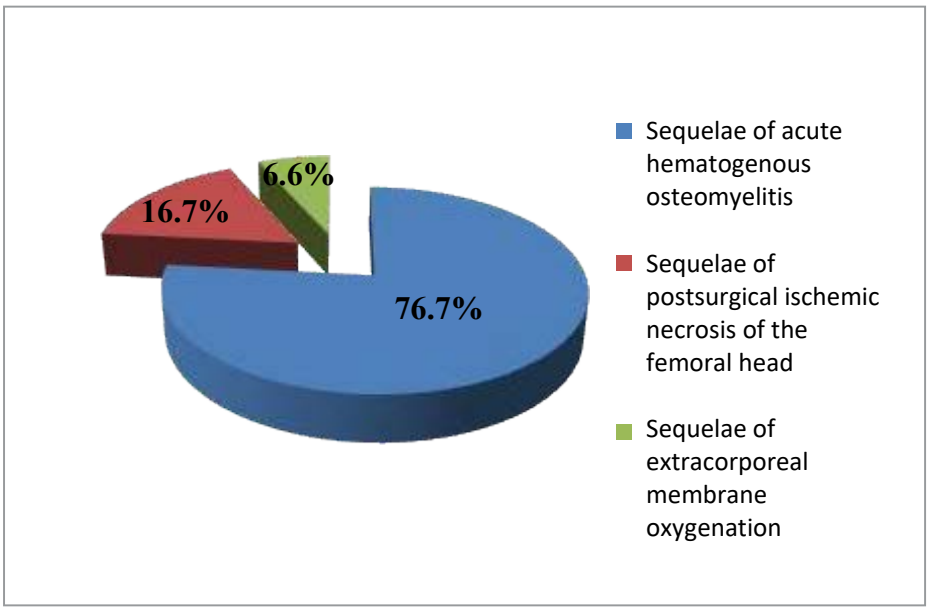

Fig. 1. High-riding greater trochanter: breakdown by etiology

Table 1

Amplitude of hip joint movements in children with bilateral high-riding greater trochanter

Movement	Amplitude (M±SD)
Flexion	110±5°
Extension	5±5°
Abduction	10±5°
Rotation	15±10°
Circumduction	45±15°

No significant (>1 cm) difference in the length of the lower limbs noted in any patient. Trendelenburg's sign bilaterally positive in all patients.

None of the patients had frontal spinal imbalance. Adams's test was negative in all children. Sagittal spinal profile altered in all patients as lumbar hyperlordosis. Table 1 shows changes in the goniometry of the affected hip joints.

Table 1 shows all the patients had limited abduction, extension, and rotation, as well as excessive circumduction in their hips. Impingement test was positive in 22 patients (73.3%) with an average VAS score of 3.4±1.5 in 18 patients (81.8%), 4.7±0.8 in 4 (18.2%). This corresponded to moderate pain syndrome.

Table 2 shows the results of X-ray tests (maxima, minima, and means of the Sharp and Wiberg angles, neck-shaft angle (NSA), angle of antetorsion (AA), TTD, CTD, hip impingement extent, TK and GLL degree, and sagittal spine-hip ratios).

Table 2 data suggests that the spatial position of the acetabulum, as well as the stability of the hip joints, was physiologically normal. The spatial orientation of the proximal femur was normal angle-wise; however, CTD was significantly different and TTD was slightly different from the norms [2; 13]. This indicated an anatomical deformity of the proximal femur: a shorter neck and a hypertrophic greater trochanter. TK was physiologically normal, but GLL exceeded the norm by far. Sagittal spine-hip ratios revealed differences in the positional indicators (lower PT and higher SS) as well as a pronounced SVA displacement posteriorly of the sacral promontory. Such change in the sagittal spine-hip ratios manifests itself as excessive pelvic anteversion and negative imbalance: Roussouly's hyperlordotic vertical posture Type IV. Correlation testing revealed a strong correlation between PI and SS ($r=0.89$; $p<0.05$), GLL and SS ($r=0.8$; $p<0.05$), see Figures 2A and 2B. Besides, there was a strong positive SS-CTD correlation ($r=0.69$; $p<0.05$), see Figure 3.

Table 2

Spatial orientation values of the acetabulum, proximal femur, hip stability, sagittal spine profile, and spine-hip ratios in children with high-riding greater trochanter as compared to normal values per literature data

Indicators	Patients with bilateral high-riding greater trochanter, M±SD (min-max)	Means in healthy children (Kamosko, 2010 [11], Hesarikia et al., 2018 [12]), M±SD
Sharp angle (°)	40.1±3.4 (34–47)	35–45
Wiberg angle (°)	32±4.4 (26–40)	25–40
HIE, %	94.3±6.5 (85–100)	85–100
NSA (°)	135.3±5.6 (122–143)	125–140
AA (°)	24±6.1 (12–36)	10–30
TTD (mm)	59.5±9.6 (43–74.5)	55.1±11.5
CTD (mm)	29.4±3.6 (21.6–34)	
PI (°)	48.4±6.4 (39.3–64.6)	45.4±10.7
PT (°)	–1.4±2.8 (–8.1–3.1)	10.3±6.5
SS (°)	49.8±5.5 (40–64)	35.4±8.1
TK (°)	35.6±4.2 (21.3–41)	37.1±9.9
GLL (°)	65.1±6.8 (56.3–87.3)	39.6±12.4
SVA (°)	–18.4±6.2 (–27.4–0)	0.1±2.3

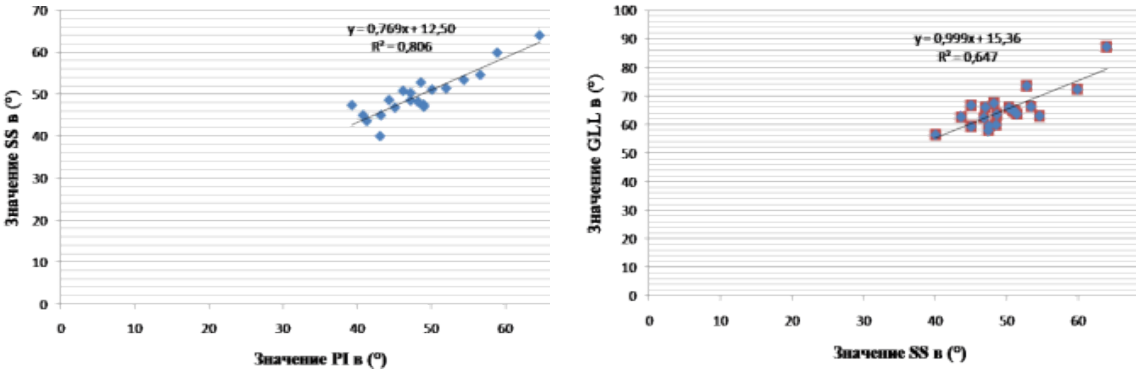

A *B*

Fig. 2. Strong correlation: A: PI and SS; B: SS and GLL;

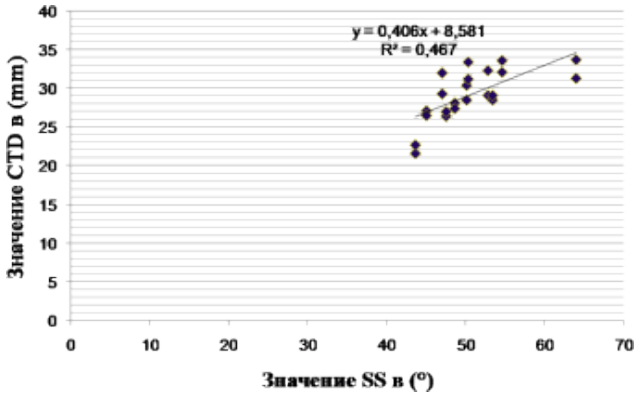

Fig. 3. Strong SS-CTD correlation

Some hip diseases are known to negatively affect the growth plates of the proximal femur, resulting in multiplane deformities. Regardless of the etiology, high-riding greater trochanter is the most common pathology, caused by damage to the growth plate of the femoral head and the upper neck edge. The person's further growth jeopardizes the anatomy and biomechanics of the hip as the gluteal muscle attachment points grow closer, which might cause extraarticular impingement later on [14]. Clinical manifestations include gluteal muscle dysfunction, gait disorders, and pain syndrome.

To assess the state of sagittal spine-hip ratios, the researchers analyzed them in comparison to healthy children of the same age category [12].

In this research, bilateral high-riding greater trochanter patients did not differ from their healthy counterparts in terms of PI. However, PT and SS, both quantifying horizontal pelvic departure, did differ significantly. PT means were significantly lower, SS means were higher. Such values of the pelvic indices point to excessive anterior rotation of the pelvis.

In this research, the key spine-hip ratios had strong correlations, which is in line with literature data [12]. Besides, this study found a strong correlation between pelvic anteversion and the height of the high-riding greater trochanter.

Mean TK did not differ significantly in affected children vs healthy children. However, GLL was nearly twice the age-appropriate value. Analysis of SVA as a global sagittal balance characteristic showed that the patients typically had their SVA displaced posteriorly of the sacral promontory by 18.4 mm on average. Thus, the category typically had negative imbalance, because a person is considered balanced as long as their SVA is displaced by <4 mm off the gravity line [15; 16].

Roussouly's (2003) classification of vertical postures in asymptomatic cohort helps predict the emergence and course of degenerative and dystrophic processes in the lumbar spine. Data collected herein corresponds to hyperlordotic vertical posture Type IV, which creates ground for anatomical change that will result in pathological burdening of the posterior spinal column, leading to 'kissing' spinous processes and in some cases to spondylolisthesis [17], see Figure 4.

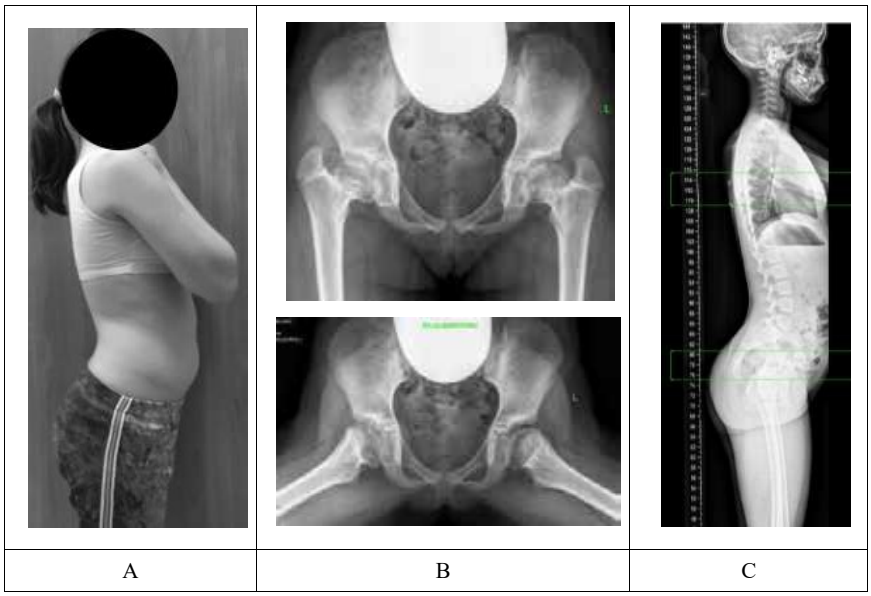

Fig. 4. Patient A, female, 13: multiplane proximal femur deformity and high-riding greater trochanter resulting from acute hematogenous osteomyelitis. A: patient's appearance showing strong lumbar lordosis; B: X-ray image of the hip joints (PA and Lauenstein projection) showing coxaplana, a shorter femoral neck and a high-riding greater trochanter on either side; C: lateral panoramic X-ray image of the spine (C1-S1) covering the femurs, showing excess pelvic rotation anteriorly and lumbar hyperlordosis

CONCLUSIONS

Children suffering from high-riding greater trochanter have a pronouncedly stronger GLL, increased SS, reduced PT, and SVA displaced posteriorly of the sacral promontory. These changes in total manifest themselves as the excessive anterior rotation of the pelvis and lumbar hyperlordosis. Such X-ray findings point to Roussouly's vertical posture Type IV (hyperlordotic posture). These X-ray-identified anatomical changes occurring during the childhood serve as a substrate for further extraarticular femoroacetabular impingement and early coxarthrosis, whilst compensatory changes in the spinal motion segments of the lumbar spine are fundamental to early degeneration and dystrophy. The results of this study call for further research to measure the post-operative change in sagittal spine-hip ratios and to find how corrective surgeries could be optimized.

CONFLICTS OF INTEREST

The authors declare no conflict of interest

The research was carried out under Government Contract of the Russian Health Ministry No. AAAA-A18-118122690158-2.

REFERENCES

1. Mazzini J.P., Martín J.R., Ciruelos R.M. Coxa vara with proximal femoral growth arrest as a possible consequence of extracorporeal membrane oxygenation: a case report. *Cases Journal*. 2009, vol. 2, no. 1, pp. 8130, doi: 10.4076/1757-1626-2-8130.

2. Pozdnikin I.Y., Baskov V.E., Barsukov D.B. Relative overgrowth of the greater trochanter and trochanteric-pelvic impingement syndrome in children: causes and X-ray anatomical characteristics. *Pediatric Traumatology, Orthopaedics and Reconstructive Surgery.* 2019, vol. 7, no. 3, pp. 15-24. doi 10.17816/PTORS7315-24.

3. Ganz R., Gill T.J., Gautier E., Ganz K., Krugel N., Berlemann U. Surgical dislocation of the adult hip a technique with full access to the femoral head and acetabulum without the risk of avascular necrosis. J. Bone Joint Surg. Br. 2001. V. 83. P. 1119-1124.

4. Leunig M., Ganz R. The evolution and concepts of joint preserving surgery of the hip. *The Bone & Joint Journal*, 2014, vol. 96-B, no. 1, pp. 5-18, doi 10.1302/0301-620x.96b1.32823.

5. De Sa D., Alradwan H., Cargnelli S. et al. Extra-articular hip impingement: a systematic review examining operative treatment of psoas, subspine, ischiofemoral, and greater trochanteric/pelvic impingement. Arthroscopy. *The Journal of Arthroscopic & Related Surgery*. 2014, vol. 30, no. 8, pp. 1026–1041, doi 10.1016/j.arthro.2014.02.042.

6. Bech N.H., Haverkamp D. Impingement around the hip: beyond cam and pincer. *EFORT Open Reviews*. 2018, vol. 3, no. 2, pp. 30-38, doi 10.1302/2058-5241.3.160068.

7. Bortulev P.I., Vissarionov S.V., Baskov V.E. et al. Clinical and roentgenological criteria of spine-pelvis ratios in children with dysplastic femur subluxation. *Traumatology and Orthopedics of Russia*. 2018, vol. 24, no. 3, pp. 74-82, doi 10.21823/2311-2905-2018-24-3-74-82.

8. Khominets V.V., Kudyashev A.L., Shapovalov V.M. et al. Modern approaches to diagnostics of combined degenerative hip and spine pathology. *Traumatology and Orthopedics of Russia*. 2014, no. 4, pp. 16-26, doi 10.21823/2311-2905-2014-0-4-16-26.

9. Albers C.E., Steppacher S.D., Schwab J.M. et al. Relative Femoral Neck Lengthening Improves Pain and Hip Function in Proximal Femoral Deformities With a High-riding Trochanter. *Clinical Orthopaedics and Related Research*. 2015, vol. 473, no. 4, pp. 1378–1387, doi 10.1007/s11999-014-4032-9.

10. Tschauner C., Graf R. Triple intertrochanteric osteotomy in coxa vara associated with high riding of the great trochanter and leg shortening. *Orthopaedics and traumatology*. 1994, vol. 3, no. 1-2, pp. 88-100, doi 10.1007/bf02620396.

11. Kamosko M.M., Baindurashvili A.G. Dysplastic coxarthrosis in children and adolescents (clinic, pathogenesis, surgical treatment) [Displasticheskii koksartroz u detei i podrostkov (klinika, patogenez, khirurgicheskoe lechenie)]. St. Petersburg, SpetsLit, 2010, 72 p.

12. Hesarikia H., Rahimnia A. Differences between male and female sagittal spinopelvic parameters and alignment in asymptomatic pediatric and young adults. *Minerva Ortopedica e traumatologica*. 2018, vol. 69, no. 2, pp. 44-48.

13. Omeroglu H., Ucar D.H., Tumer Y.A new measurement method for the radiographic assessment of the proximal femur: the center-trochanter distance. *Acta Orthopaedica et Traumatologica Turcica*. 2004, vol. 38, no. 4, pp. 261-264.

14. Leunig M, Ganz R. Relative neck lengthening and intracapital osteotomy for severe Perthes and Perthes-like deformities. *Bull NYU HospJtDis*. 2011, vol. 69, suppl. 1, pp. 62-67.

15. Ozer A.F. Kaner T., Bozdogan C. Sagittal Balance in the Spine. *Turkish Neurosurgery*. 2014. vol. 24, no. 1, pp. 13-19.

16. Zheng X., Chaudhari R., Wu C. et al. Repeatability test of C7 plumb line and gravity line on asymptomatic volunteers using an optical measurement technique. *Spine*. 2010, vol. 35, no. 18, p. E889-E894, doi 10.1097/brs.0b013e3181db7432.

17. Jackson R., Phipps T., Hales C. et al. Pelvic lordosis and alignment in spondylolisthesis. *Spine*. 2003, vol. 28, no. 2, pp. 151-160, doi 10.1097/00007632-200301150-00011.

PROGNOSTIC VALUE OF THE MUCIN IMMUNOHISTOCHEMICAL PROFILE OF EARLY GASTRIC CANCER

Mochalnikova V.V.[1], Gorsheneva V.M.[2], Perevoschikov A.G.[1], Malikhova O.A.[1, 3]

[1]Federal State Budgetary Institution «N.N. Blokhin National Medical Research Center of Oncology» of the Ministry of Health of the Russian Federation, Moscow, e-mail: mochalnikova70@yandex.ru;

[2]ANO "Central Clinical Health Unit" of the Russian Federation, Magnitogorsk, e-mail: venera_gorshenev@mail.ru;

[3]Russian Medical Academy of Continuous Professional Education of the Ministry of Health of the Russian Federation, Moscow, e-mail: malikhova@inbox.ru

The mucin immunohistochemical profile of early gastric cancer (EGC) has certain clinicopathological features that are independent of the histological type of the tumour. In this study, we identified the prevalence and prognostic value of the mucin profile of EGC.

Aims

The aim of the study was to compare the mucin profile variants based on clinicopathological characteristics and histological type of early gastric cancer (EGC).

Materials and Methods

Immunhistochemistry analysis was performed on the surgical material of 227 cases of EGC, with testing the expression of marker mucins MUC 5 AC, MUC6, MUC2, and CD10. The mucin immunophenotype variants were classified as gastric, intestinal, mixed, and null immunophenotype according to the immunopositivity of the above markers.

Results

EGC with the gastric immunophenotype was characterised by more aggressive morphological features – it occurred significantly more often (compared to the intestinal phenotype) in the 0 III macroscopic type, ulcerated type, K. Nakamura undifferentiated histological type, in P. Lauren diffuse type, and JGCA signet ring cell histological type of EGC. Also, EGC with the gastric immunophenotype showed a higher rate of metastasis compared to the intestinal one (20.6% vs. 11.7%), and the metastasis rate in differentiated EGC with the gastric immunophenotype were notably higher than in the intestinal one (9/2; 22.3% vs. 40/3; 7.0%), but the data did not reach significance due to the small sample size. EGC with the intestinal immunophenotype had more favourable morphological features and was significantly more common with intramucosal localisation, 0 I macroscopic type, K. Nakamura differentiated type, P. Lauren intestinal type, and JGCA highly differentiated adenocarcinoma, and had the lowest incidence of ulceration.

Conclusions

The results suggest that the mucin profile of EGC is associated with tumour progression. The gastric immunophenotype of EGC was associated with more aggressive morphological characteristics than the intestinal one.

Keywords: early gastric cancer, mucin immunophenotype

INTRODUCTION

Early gastric cancer (EGC) is characterized by high heterogeneity. However, histological classifications such as Lauren P. [1] and Japanese Gastric Cancer Association (JGCA) (2014) [2] classifications and the classification of Nakamura K. [3] that provides grounds for the indication of endoscopic JGCA resection [4], do not reflect all the clinical and prognostic peculiarities of EGC. Taking into account the presence of minimal risk for lymphogenic metastasizing in cases that meet the extended indications for endoscopic JGCA resection, there is a necessity for additional methods for evaluating the malignant potential of EGC in order to verify the risk of lymphogenic metastasizing and help to choose the treatment tactics. The mucin profile of EGC is an important immune histochemical marker of the disease prognosis. Mucins are glycosylated glycoproteins that look like a cohesive gel secreted by the epithelium of the gastrointestinal tract. The identification of the mucin profile (immune phenotype) of EGC is based on the immune histochemical establishment of the expression of markers to mucins of normal epithelial cells of the

gastrointestinal tract in tumor cells. According to a traditional classification [5, 6], the mucin profile of EGC is divided into 4 variants: intestinal (expression of the minimum one of the intestinal markers MUC 2, CD 10), gastric (expression of the minimum one of the gastric markers MUC 5 AC, MUC 6), mixed (a combination of expression of gastric and intestinal markers), and null (non-classified – no expression). It is known that variants of the mucin immune phenotype of EGC are spread significantly and associated with malignant potential. However, the data on the association between the mucin profile of EGC and tumor behavior are controversial [7, 8].

The study was aimed to perform a comparative evaluation of the variants of the mucin profile depending on the clinical-morphological characteristics and histological type of EGC. The authors believe that the identification of the mucin immune histochemical profile of EGC as a prognostic factor can be an integral part of the preoperational stage of patients' examination for the choice of treatment tactics.

MATERIALS AND METHODS

General characteristics. The authors conducted a retrospective study that included operational material obtained from 277 patients with EGC (113 (49.8%) males and 114 (50.2%) females) that underwent radical surgery with a lymph node dissection at the department of abdominal surgery of the N.N. Blokhin National Medical Research Center of Oncology. The volume of surgery and the level of lymph node dissection were estimated according to the JGCA recommendations [4]. The mean age of patients was 58.5±11.4 years old (from 26.4 to 90 years old, median 59 years).

Histological study. The operational material (hematoxylin-eosin stained microslides) was retrospectively studied by two pathologists and reclassified according to the histological classification of tumors using Lauren P. [1], Nakamura K. [3], and JGCA 2014 classifications [2].

Immunohistochemical study. An immunohistochemical study was performed by a peroxidase-antiperoxidase method on waxed 5 μm sections according to a standard protocol. The authors used the most representative waxed block of the operational material obtained from 227 patients with EGC (monoclonal antibodies to mucins MUC 5 AC, MUC 6, MUC 2 – Novocastra, CD10 – DAKO). The expression of MUC 5 AC, MUC 6, MUC 2, and CD10 was evaluated depending on the intensity of staining. The criteria for positive expression of markers to mucins were 20% of stained tumor cells and 10–5% of CD 10 positive cells [9]. For internal control, non-tumor gastric mucosa was used. The percentage of positively stained cells was estimated by two independent pathologists. The discrepancy in the interpretation of the estimation was solved based on consensus. Cases of EGC were divided into four mucin immune phenotypes: gastric, intestinal, mixed, and null based on the recommendations [5, 6].

Statistical analysis. The statistical analysis of the obtained data and calculation of the parameters were performed in Microsoft Excel, Statistica for Windows v.10, and SPSS v.21. Continuous variables were compared using Student's t-test or Mann-Whitney U-test. Categorical variables were compared using Chi-square or Fisher's exact test. The differences were considered significant at $p<0.05$.

RESULTS

General characteristics of the mucin profile of EGC (n=227). Patients with EGC with the gastric immune phenotype were significantly younger (the mean age of patients was 55.6±11.4 years old in comparison with the null immune phenotype (p=0.046) and intestinal immune phenotype (p=0.038)). In the group of patients with the gastric immune phenotype, the share of patients older than 60 years old (35.3%) was significantly lower than in the group with the intestinal immune phenotype (50.0%) and null immune phenotype (55.6%) (p=0.038). In patients with the intestinal immune phenotype, tumors with intramucosal localization prevailed (70%) (p=0.023) in comparison with the null immune phenotype (47.2%). The lowest rate of occurrence was observed in tumors with the depth of invasion SM 2–10.0% (p=0.049) in comparison with the null immune phenotype (25.0%). In patients with the gastric immune phenotype, tumors with ulceration were observed significantly more often 48.5% (p=0.025) in

comparison with the intestinal phenotype (30.0%), 0 IIc macroscopic type (38.2%) (p=0.018) in comparison with the null phenotype (16.7%), and 0 III macroscopic type (25.0%) (p=0.043) in comparison with the intestinal phenotype (11.7%). In patients with EGC of gastric immune phenotype, a higher rate of metastasizing was observed than in patients with the intestinal immune phenotype (20.6% versus 11.7%). The highest rate of lymphogenic metastasizing was revealed in patients with the null immune phenotype.

Variants of the mucin immune phenotype of EGC did not have significant differences by the localization and maximal size of the tumor and the presence of lymph-vascular invasion. A detailed characteristic of the variants of the mucin immune phenotype of EGC (n=227) is presented in Table 1.

Table 1

Characteristics of the variants of mucin immune phenotypes in the group of patients with EGC (n=227)

		Mucin immune phenotypes							
		null		gastric		intestinal		mixed	
N		36		68		60		63	
		abs.	%	abs.	%	abs.	%	abs.	%
Sex	male	19	52.8	29	42.6	32	53.3	33	52.4
	female	17	47.2	39	57.4	28	46.7	30	47.6
Age	< 60 years old	16	44.4	44	64.7	30	50.0	37	58.7
	> 60 years old	20	55.6	24	35.3*	30	50.0	26	41.3
Ulceration and fibrosis	no	21	58.3	35	51.5	42	70.0	34	54.0
	yes	15	41.7	33	48.5+	18	30.0	29	46.0+
Lymph-vascular invasion	no	31	86.1	62	91.2	52	86.7	52	82.5
	yes	5	13.9	6	8.8	8	13.3	11	17.5
Depth of invasion	M	17	47.2	41	60.3	42	70.0*	35	55.6
	SM1	10	27.8	18	26.5	12	20.0	15	23.8
	SM2	9	25.0	9	13.2	6	10.0*	13	20.6
Localization	L and LD	14	38.9	34	50.0	31	51.7	31	49.2
	M and ML.	16	44.4	27	39.7	22	36.7	26	41.3
	U all with E -	5	13.9	5	7.4	4	6.7	3	4.8
	U (E+)	1	2.8	2	2.9	3	5.0	3	4.8
Macroscopic type	0 I	19	52.8	7	10.3*+	17	28.3*	12	19.0*
	0 II a	1	2.8	11	16.2*	13	21.7*	7	11.1
	0 II b	4	11.1	7	10.3	3	5.0	9	14.3
	0 II c	6	16.7	26	38.2*	20	33.3	25	39.7*
	0 III	6	16.7	17	25.0+	7	11.7	10	15.9
N+		8	22.2	14	20.6	7	11,7	9	14,3
Maximum size		2.97±1.59		2.98±1.50		2.64±1.46		2.48±1.39	
Mean age		60.4±11.5		55.6±11.4*+		59.6±9.7		59.6±12.3	

*Significant differences in comparison with the null phenotype, p<0.05.
+ Significant differences in comparison with the intestinal phenotype, p<0.05.

Mucin profile of EGC in respect to the morphological characteristics of the tumor

The distribution of the variants of the mucin immune phenotype with respect to the tumor size.

The variants of the mucin immune phenotype did not correlate with the maximal size of the tumor (Table 1). However, it should be noted that among minor tumors (1–2 cm), a mixed immune phenotype of EGC prevailed (33.7%). Along with an increase in the tumor size (2.01–3 cm and >3 cm), the number of cases with the mixed immune phenotype decreased (25.0% versus 22.1%) and the number of cases with null immune phenotype insignificantly decreased (M – 13.3%, SM 1 – 15.4%; SM2 – 19.5%).

The characteristic of the variants of the mucin immune phenotype with respect to the depth of invasion of EGC

The intestinal immune phenotype was more often observed in cases with intramucosal EGC (31.1%) and significantly rarer in cases with the depth of invasion SM2 (16.2%; p=0.053). *The gastric immune phenotype* in cases with intramucosal EGC was met rarer (30.4%) than intestinal but the rate of occurrence did not change with an increase in the depth of tumor invasion unlike the intestinal immune phenotype (SM1 – 32.7%; SM 2 – 24.3%). In cases with intramucosal EGC, the *null immune phenotype* (12.6%) was observed significantly rarer than the other phenotypes (gastric p=0.0003, intestinal p=0.0002, mixed p=0.004). In cases with a maximal depth of invasion SM2, the *mixed immune phenotype* was observed two times more often than intestinal (35.1%; p=0.055) (Table 2).

The characteristics of the variants of the mucin immune phenotype of EGC with respect to a macroscopic type of tumor

The gastric immune phenotype was observed significantly more often in cases with 0III macroscopic type (42.5%; p=0.014 in comparison with intestinal 17.5%). The lowest occurrence rate of the gastric immune phenotype was observed in cases with 0I macroscopic type (12.7%) (data were significant in comparison with the null immune phenotype (34.5%; p=0.006) and intestinal immune phenotype (30.9%; p=0.018). *The intestinal immune phenotype* was met significantly more often in cases with 0I and 0II macroscopic type (in comparison with gastric 30.9%; p=0.018 and null 40.6%; p=0.0002). The lowest occurrence rate of this immune phenotype was observed in cases with 0III macroscopic type 17.5% (in comparison with gastric; p=0.014).

The association between the mucin immune phenotype of EGC with ulceration. In cases with EGC with ulceration, the gastric phenotype was met significantly more often (34.7%) in comparison with intestinal 18.9% (p=0.011) and null 15.8% (p=0.002). In cases with non-ulcerous EGC, the rate of occurrence of the intestinal immune phenotype (31.8%) was significantly higher than in cases with ulcerous cancer (18.9%, p=0.021).

Table 2

Characteristics of the variants of the mucin immune phenotype of EGC depending on the depth of the invasion

Mucin phenotype	Depth of invasion							
	M		SM1		SM2		Total	
Number of patients	135		55		37		227	
	Abs	%	Abs	%	Abs	%	Abs	%
null	17	12.6	10	18.2	9	24.3	36	15.9
gastric	41	30.4*	18	32.7	9	24.3	68	30.0
intestinal	42	31.1*	12	21.8	6	16.2	60	26.4
mixed	35	25.9*	15	27.3	13	35.1	63	27.8

*Significant changes in comparison with null phenotype, p<0.05

Table 3

Characteristics of the mucin profile of EGC depending on the Lauren classification

	Intestinal		Diffuse		Mixed		Total	
Number of patients	123		72		32		227	
	Abs.	%	Abs.	%	Abs.	%	Abs.	%
null	25	20.3	10	13.9	1	3.1	36	15.9
gastric	13	10.6	43	59.7*#	12	37.5*#	68	30.0
intestinal	51	41.5*+	4	5.6	5	15.6	60	26.4
mixed	34	27.6	15	20.8	14	43.8*#	63	27.8

*Significant differences in comparison with the null phenotype, p<0.05
+Significant differences in comparison with the gastric phenotype, p<0.05 #Significant differences in comparison with the intestinal phenotype, p<0.05

Table 4

Characteristic of the mucin profile of the differentiated and non-differentiated types of EGC

	Differentiated type		Non-differentiated type		Total	
Number of patients	91		136		227	
	Abs.	%	Abs.	%	Abs.	%
null	13	14.3#	23	16.9+	36	15.9
gastric	9	9.9#	59	43.4*	68	30.0
intestinal	43	47.3	17	12.5*+	60	26.4
mixed	26	28.6#	37	27.2+	63	27.8

*Significant differences between the types by the Nakamura classification, p<0.05
+Significant differences in comparison with the gastric phenotype, p<0.05
Significant differences in comparison with the intestinal phenotype, p<0.05

The Lauren classification [1]. In the general sampling (n=227), more than half of cases of EGC had intestinal type (intestinal – 54.1%; diffuse – 31.7%; mixed – 14.2%; p=0.00001). The intestinal type of EGC was not completely represented by the intestinal immune phenotype. Still, this mucin profile prevailed (41.5% of cases) in comparison with the gastric phenotype (10.6%; p=0.00001) and null phenotype (20.3%; p=0.0003). In half of the cases, the diffuse type of EGC had the gastric immune phenotype (59.7%) in comparison with intestinal (5.6%; p=0.00001) and null (13.9%; p=0.00001). In cases with mixed histological type, the mixed phenotype prevailed (43.8%) in comparison with the intestinal (p=0.014) and null (p=0.0001) phenotypes and the gastric phenotype (37.5%) prevailed in comparison with the null (3.1%) (p=0.0006) and intestinal (15.6%) (p=0.044). (Table 3).

Histological classification by Nakamura K. [3]. In cases with differentiated type by the classification of Nakamura, the *intestinal phenotype* was observed significantly more often (47.3%; (p=0.00001 in comparison with gastric, p=0.00001 – null, p=0.007 – mixed). In cases with non-differentiated type, the *gastric immune phenotype* prevailed (43.4%; p=0.00001 in comparison with null, p=0.00001 – intestinal, p=0.004 – mixed). The comparison of histological types in cases of a differentiated type showed that the intestinal immune phenotype (p=0.00001) was observed more often than in cases of a non-differentiated type; in cases of a non-differentiated type, gastric phenotypes prevailed (p=0.00001) (Table 4).

The study of regional metastasizing in cases of a differentiated type of EGC with the gastric immune phenotype showed that the rate of metastasizing was significantly higher (9/2; 22.3%) than in cases with the intestinal phenotype (43/3; 7.0%). However, these data did not meet the criterion of significance because of a small sampling. In cases with a non-differentiated type, the rate of lymphogenic metastasizing in patients with EGC with the gastric and intestinal immune phenotypes was similar (20.3% and 23.5%, respectively).

Histological classification JGCA 2014 [2]. *The intestinal immune phenotype* was observed significantly more often in cases with highly differentiated adenocarcinoma (more than in half of the cases – 58.6). Along with a decrease in the differentiation of EGC, the number of cases with the intestinal immune phenotype decreased (non-solid low-differentiated adenocarcinoma (17.1%; p=0.00001), solid low-differentiated adenocarcinoma (20.0%; p=0.027), colloid cancer (4.2%; p=0.00001). On the contrary, the *gastric immune phenotype* was rarely met in cases with highly-differentiated adenocarcinoma (3.4%) but significantly more often in cases with the colloid histological type of EGC (70.4%; p=0.00001 in comparison with highly differentiated adenocarcinoma – 3.4%, p=0.0001 in comparison with moderately differentiated adenocarcinoma – 17.6%, p=0.003 in comparison with low differentiated solid adenocarcinoma – 20.0%, p=0.00001 with low differentiated non-solid adenocarcinoma – 14.6%, p=0.00001 with papillary adenocarcinoma – 18.2%).

The null immune phenotype was observed in cases with such an unfavorable type of cancer as low differentiated solid adenocarcinoma (50%) (in comparison with highly differentiated adenocarcinoma – 8.6% (p=0.004), moderately differentiated adenocarcinoma – 5.9% (p=0.015), colloid cancer – 7.0% (p=0.0019), and papillary adenocarcinoma – 40.9% (in comparison with highly differentiated adenocarcinoma – 8.6% (p=0.0017), moderately differentiated adenocarcinoma – 5.9% (p=0.014), colloid cancer – 7.0% (p=0.0005)).

The morphological characteristics of the tumor that provided grounds for the evaluation of the risk of lymphogenic metastasizing in patients with EGC and indications for endoscopic resection cannot be precisely identified during the preoperative examination of a patient [10-12]. Besides, the expanded indications for endoscopic resection in patients with EGC are not always safe [13]. The authors believe that such an additional factor of prognosis of the progression of EGC as a mucin profile of the tumor can help in the choice between EGC endoscopic resection and surgical operation.

The majority of the studies on the mucin profile of EGC were conducted in Asian countries. The present study was one of the first in Russia. It showed that the rate of occurrence of the variants of mucin immune phenotypes in the general sampling (n=227) was uniform (intestinal – 26.40%, gastric – 30.00%, mixed – 27.80%, null – 15.90%). The intestinal type of carcinoma by the classification of Lauren and the differentiated type by the classification of Nakamura K. were characterized not only by an intestinal immune phenotype but also gastric, mixed, and null mucin phenotypes, which agreed with the available published data [5, 6, 9]. According to the published data, an increase in the size of the tumor and depth of invasion led to a phenotypic shift in the mucin profile of EGC from the gastric to intestinal immune phenotype [14, 15]. On the contrary, some other studies showed that the number of cases with gastric and intestinal immune phenotypes increased and the number of cases with mixed mucin phenotype decreased ($p < 0.05$) [16]. The present study showed that an increase in the size and depth of tumor invasion led to an insignificant increase in the number of cases with the gastric immune phenotype and a decrease in the number of cases with intestinal immune phenotypes.

It is known that the intestinal and gastric immune phenotypes of EGC have different occurrence rates and are associated with different malignization potential. However, these data on the association of mucin immune phenotypes with tumor behavior are controversial [14]. The majority of researchers believe that the gastric immune phenotype of EGC is prognostically more unfavorable than intestinal. The authors report on a significantly deeper invasion, a higher rate of lymphovascular invasion and ulceration, a higher rate of venous invasion, and metastasizing into regional

lymph nodes in cases with the gastric immune phenotypes of EGC in comparison with intestinal [8, 17, 18]. In the present study, EGC with gastric immune phenotype was also characterized by more aggressive morphological features. It correlated with 0 III macroscopic type, ulceration, and low differentiated histological type. Besides, in cases of EGC with the gastric immune phenotype, a higher level of metastasizing was observed in comparison with intestinal (20.6% and 11.7%, respectively). On the contrary, the intestinal phenotype was revealed significantly more often in cases with intramucosal EGC (depth of invasion M – 70%, p=0.023; depth of invasion SM 2–10%; p=0.049) and highly differentiated histological type, which agreed with the available published data [7, 18, 19].

Besides, EGC of a differentiated type by the classification of Nakamura K. [3] with the gastric immune phenotype has unique characteristics that distinguish it from differentiated EGC with the intestinal immune phenotype because of higher malignization potential and tendency to metastasize. It is noted that EGC with the gastric mucin immune phenotype has a larger diameter and deeper invasion of a submucosal layer than the intestinal phenotype [17, 18]. Besides, it is more often observed in cases with colloid cancer and tends to a faster transformation into a non-differentiated type, ulceration, and metastasizing at the initial stage of cancerogenesis [9, 20]. According to the published data, the rate of occurrence of the gastric immune phenotype in cases with differentiated EGC varied from 7.9% to 23.9% [14, 21] and could reach 52.38% [9]. In the present study, in cases with a differentiated type of EGC, the gastric immune phenotype was observed in 9.8% of cases (9/91), intestinal – in 47.2% (43/91). The importance of the study of the mucin profile of EGC is explained by the fact that differentiated EGC (by the classification of Nakamura), especially with a diameter < 2 cm, is a generally accepted criterion of the indication for endoscopic resection of EGC proposed by JGCA [4]. The results of the present study showed that in cases with differentiated EGC with gastric immune phenotype, the rate of metastasizing was significantly higher than with intestinal (22.3% and 7.0%, respectively).

CONCLUSIONS

The authors believe that the gastric immune phenotype of EGC is an unfavorable prognostic feature. For this reason, the identification of the mucin profile of EGC can become an additional prognostic factor for the choice of treatment tactics for EGC. The immunohistochemical identification of the mucin profile of EGC is a simple and cheap method that can help specify and expand the indications for endoscopic resection of EGC.

CONFLICTS OF INTEREST

The authors declare no conflict of interest

REFERENCES

1. Lauren P. The two histological main types of gastric carcinoma: diffuse and so-called intestinal-type carcinoma. An attempt at a histo-clinical classification. *Acta Pathologica Microbiologica Scandinavica*. 1965, vol. 64, no. 1, pp. 31–49, doi: 10.1111/apm.1965.64.1.31

2. Japanese Gastric Cancer Association. Japanese classification of gastric carcinoma: 3rd English edition. *Gastric Cancer*. 2011, vol. 14, no. 2, pp. 101–112, doi 10.1007/s10120-011-0041-5.

3. Nakamura K, Sugano H, Takagi K. Carcinoma of the stomach in incipient phase: its histogenesis and histological appearances. *Gann*. 1968, vol. 59, pp. 251–258.

4. Japanese Gastric Cancer Association. Japanese gastric cancer treatment guidelines 2014 (ver. 4). *Gastric Cancer*. 2017, vol. 20, no. 1, pp. 1-19, doi 10.1007/s10120-016-0622-4.

5. Shiroshita H., Watanabe H., Ajioka Y. et al. Re-evaluation of mucin phenotypes of gastric minute well-differentiated-type adenocarcinomas using a series of HGM, MUC5AC, MUC6, M-GGMC, MUC2 and CD10 stains. *Pathology International*. 2004, vol. 54, no. 5, pp. 311–321, doi: 10.1111/j.1440-1827.2004.01625.x.

6. Sugai T., Tsukahara M., Endoh M. et al. Analysis of cell cyclerelated proteins in gastric intramucosal differentiated-type cancers based on mucin phenotypes: a novel hypothesis of early gastric carcinogenesis based on mucin phenotype. *BMC Gastroenterology*. 2010, vol. 10, no. 1, p. 55., doi 10.1186/1471-230x-10-55.

7. Hondo F.Y., Kishi H., Safatle-Ribeiro A.V. et al. Characterization of the mucin phenotype can predict gastric cancer recurrence after endoscopic mucosal resection. *Arquivos de Gastroenterologia*. 2017, vol. 54, no. 4, pp. 308-314, doi 10.1590/s0004-2803.201700000-38.

8. Han J.P., Hong S.J., Kim H.K. et al. Expression of immunohistochemical markers according to histological type in patients with early gastric cancer. *Scandinavian Journal of Gastroenterology*. 2016, vol. 51, no. 1, pp. 60-66, doi 10.3109/00365521.2015.1065510.

9. Cavalcanti E., De Michele F., Lantone G. et al. Mucin phenotype of differentiated early gastric cancer: an immunohistochemistry study supporting therapeutic decision making. *Cancer Management and Research*. 2019, vol. 11, pp. 5047-5054, doi 10.2147/CMAR.S193994.

10. Nakagawa M., Choi Y.Y., An J.Y. et al. Difficulty of predicting the presence of lymph node metastases in patients with clinical early stage gastric cancer: a case control study. *BMC Cancer*. 2015, vol. 15, no. 1, pp. 943, doi 10.1186/s12885-015-1940-3.

11. Bok G.H., Kim Y.J., Jin S.Y. et al. Endoscopic submucosal dissection with sentinel node navigation surgery for early gastric cancer. *Endoscopy*. 2012, vol. 44, no. 10, pp. 953–956, doi 10.1055/s-0032-1310162.

12. Cardoso R., Coburn N., Seevaratnam R. et al. A systematic review and meta-analysis of the utility of EUS for preoperative staging for gastric cancer. *Gastric Cancer*. 2012, vol. 15, suppl. 1, pp. 19–26, doi 10.1007/s10120-011-0115-4.

13. Abdelfatah M.M., Barakat M., Lee H. et al. The incidence of lymph node metastasis in early gastric cancer according to the expanded criteria in comparison with the absolute criteria of the Japanese Gastric Cancer Association: a systematic review of the literature and meta-analysis. *Gastrointestinal Endoscopy*. 2017, vol. 87, no. 2, pp. 338–347, doi 10.1016/j.gie.2017.09.025.

14. Kabashima A., Yao T., Maehara Y. et al. Relationship between biological behavior and phenotypic expression in undifferentiated-type gastric carcinomas. *Gastric Cancer*. 2005, vol. 8, pp. 220–227, doi 10.1007/s10120-005-0340-9.

15. Tajima Y., Yamazaki K., Makino R. et al. Gastric and intestinal phenotypic marker expression in early differentiated-type tumors of the stomach: clinicopathologic significance and genetic background. *Clinical Cancer Research*. 2006, vol. 12, no. 21, pp. 6469– 6479.

16. Ikarashi S., Nishikura K., Ajioka Y. et al. Re-evaluation of phenotypic expression in undifferentiated-type early adenocarcinonmas using mucin core pretein and CDX2. *Gastric Cancer*. 2013, vol. 16, pp. 208–219, doi 10.1007/s10120-012-0172-3.

17. Koseki K., Takizawa T., Koike M. et al. Distinction of differentiated type early gastric carcinoma with gastric type mucin expression. *Cancer*. 2000, vol. 89, no. 4, pp. 724-732, doi 10.1002/1097-0142(20000815)89:4<724::aid-cncr2>3.0.co;2-4.

18. Namikawa T., Hanazaki K. Mucin phenotype of gastric cancer and clinicopathology of gastric-type differentiated adenocarcinoma. *World journal of gastroenterology*. 2010, vol. 16, no. 37, p. 4634, doi 10.3748/wjg.v16.i37.4634.

19. Hayakawa M., Nishikura K., Ajioka Y. et al. Re-evaluation of phenotypic expression in differentiated-type early adenocarcinoma of the stomach. *Pathology International*. 2017, vol. 67, no. 3, pp. 131–140, doi 10.1111/pin.12506.

20. Hondo F.Y., Kishi H., Safatle-Ribeiro A.V. et al. Characterization of the mucin phenotype can predict gastric cancer recurrence after endoscopic mucosal resection. Arq. Gastroenterol. 2017. V. 54(4). P. 308-314. DOI: 10.1590/s0004- 2803.201700000-38.

21. Huang Q., Zou X. Clinicopathology of early gastric carcinoma: an update for pathologists and gastroenterologists. *Gastrointestinal Tumors*. 2017, vol. 3, no. 3-4, pp. 115–124, doi 10.1159/000456005.